



Licentiate Thesis in Land and Water Resources Engineering

Analysing the effect of tree canopy and urban form on urban surface heat using street IR imagery

ELINA MERDYMSHAEVA

KTH ROYAL INSTITUTE OF TECHNOLOGY



Analysing the effect of tree canopy and urban form on urban surface heat using street IR imagery

ELINA MERDYMSHAEVA

Academic Dissertation which, with due permission of the KTH Royal Institute of Technology, is submitted for public defence for the Degree of Licentiate of Engineering on Monday the 15th of June 2026, at 1:00 p.m. in H1, Teknikringen 33, Stockholm.

Licentiate Thesis in Land and Water Resources Engineering
KTH Royal Institute of Technology
Stockholm, Sweden 2026

© Elina Merdymshaeva

© Paper 1: Simone Mora, Yuki Machida, Fan Zhang, Fabio Duarte, Sanjana Paul, Carlo Ratti, Ulla Mörtberg.

© Paper 2: Shadaab Ghani, Fredrik Lindberg, Simone Mora, Ravish Dubey, Lukas Ljungqvist, Anne Håkansson,
Ulla Mörtberg.

Cover page photo: Elina Merdymshaeva

TRITA-ABE-DLT-2618

ISBN 978-91-8106-639-5

Printed by: Universitetservice US-AB, Sweden 2026

This thesis is dedicated to all the people who have supported me throughout my studies. Thanks to my supervisors, my family, partner and dear friends. Your belief in me helped me to get here, I am forever grateful and in debt for the fact that you were near.

Lastly, I want to dedicate it to my younger self. This was quite a road, but you managed. Thank you for the decision to start and finish this challenge.

Abstract

Urban heat island (UHI) effects are intensifying due to climate change and urbanisation, posing increasing risks to human health, energy demand, and environmental sustainability. Understanding how urban morphology and vegetation influence thermal conditions at street level remains challenging due to the limited spatial resolution of traditional measurement approaches. This thesis investigates urban heat dynamics in Stockholm using opportunistic drive-by sensing (DS) combined with spatial machine learning methods to analyse hyperlocal relationships between urban form, tree canopy, and surface temperature within the urban canopy layer.

High-resolution air and surface temperature data were collected during the summers of 2021 and 2022 using DS platforms mounted on electric vehicles, generating more than one million spatially distributed observations. These data were integrated with geospatial datasets describing urban morphology, greenery, and water bodies. Relationships between environmental variables and thermal patterns were analysed using statistical methods and machine learning models, including XGBoost and GPBoost, across multiple spatial scales.

The results demonstrate that DS measurements capture substantial hyperlocal variability in surface temperature that is not fully captured by weather stations or satellite-derived land-surface temperatures. Surface temperatures were generally higher and more spatially heterogeneous than air temperature, reflecting strong dependence on immediate land cover and urban geometry. Tree canopy and reduced sun exposure were consistently associated with lower surface temperature differences, while higher building density increased heat accumulation. Machine learning models showed the highest explanatory power at a hyperlocal scale, with GPBoost outperforming XGBoost due to its ability to account for spatial dependencies.

The findings highlight the importance of integrating fine-scale sensing with advanced spatial modelling to improve understanding of urban heat processes. The proposed methodological framework supports evidence-based urban planning strategies to enhance climate resilience through vegetation, shading, and urban design.

Keywords

Urban heat island, surface temperature, drive-by sensing, machine learning, tree canopy, urban morphology

Sammanfattning

Urbana värmeöeffekter (Urban Heat Island, UHI) förstärks i takt med klimatförändringar och urbanisering, vilket medför ökade risker för hälsa, energianvändning och urban hållbarhet. Trots omfattande forskning kvarstår betydande kunskapsluckor kring hur urban morfologi och vegetation påverkar temperaturförhållanden på detaljerad rumslig skala i det urbana landskapet. Denna licentiatavhandling syftar till att analysera urbana värmemönster i Stockholm med särskilt fokus på samspelet mellan bebyggelsestruktur, trädskikt och yttemperatur, genom användning av högupplöst mobil datainsamling och rumslig maskininlärning.

Studien baseras på mobil datainsamling (drive-by sensing), där temperaturdata samlats in med sensorer monterade på eldrivna fordon under somrarna 2021 och 2022. Datamaterialet omfattar över en miljon observationer av lufttemperatur och yttemperatur, vilka har integrerats med geodata om bebyggelse, vegetation och vatten. Samband mellan miljövariabler och temperaturmönster analyserades med statistiska metoder samt maskininlärningsmodeller, främst XGBoost och GPBoost, på flera rumsliga skalor.

Resultaten visar att DS-metoden möjliggör analys av betydande hyperlokal variation i yttemperatur, som inte fångas av traditionella väderstationer eller satellitbaserade observationer. Yttemperaturen uppvisar större variation och generellt högre värden än lufttemperaturen, vilket speglar stark påverkan från lokala markegenskaper och urban geometri. Trädskikt och minskad solexponering är konsekvent associerade med lägre temperaturdifferenser, medan hög bebyggelsetäthet bidrar till ökad värmeackumulering. Maskininlärningsmodellerna uppvisar högst förklaringsgrad på hyperlokal skala, där GPBoost presterar bättre än XGBoost genom att explicit beakta rumsliga beroenden.

Avhandlingen visar att kombinationen av högupplöst mobil miljömätning och avancerad rumslig modellering ger förbättrade möjligheter att förstå urbana värmeprocesser. Resultaten understryker vikten av finupplöst analys för att identifiera lokala värmemönster som är relevanta för mänsklig exponering. Den föreslagna metodansatsen bidrar till utvecklingen av evidensbaserade planeringsstrategier för klimatanpassning, där vegetation, skuggning och

urban form utgör centrala komponenter för att minska värmebelastning i städer.

Nyckelord:

Urbana värmeeffekter, ytemperatur, mobil datainsamling, maskininlärning, trädskikt, urban morfologi

Acknowledgments

I would like to thank ElectriCITY, Senseable Stockholm Lab, MIT and the City of Stockholm for the amazing collaboration throughout the years. Without your valuable input, this thesis would be incomplete.

The gratitude is largely extended to my main supervisor, Ulla Mörtberg. Thank you for your continuous support and helping me to navigate the world of academia. Without your words of encouragement and belief in me it would have been much harder to make this come to life. Beyond scientific guidance, you have always been a person who would help me out in times of struggle.

Moreover, thanks to my co-supervisor, Anne Håkansson. Your positive outlook on things and ability to explain areas that were new for me have provided me with deeper knowledge and understanding of the world of Artificial Intelligence.

Thanks to Fredrik Lindberg who joined our scientific team at the later stages. You helped to highlight the details, provided us with interesting ideas and encouraged us to go deeper into the investigation into urban heat.

I am forever grateful to my PhD colleagues and friends, Sigge, Shadaab and Zoé, for always being there for me in both good and bad. This is as well extended to non-PhD colleagues Xi-Lillian and Oleksii: with your help I learnt how to teach and how to push through busy periods.

I would also like to thank my outside-of-academia friends, Valeriia and Khrystyna. With you I learnt how to survive and endure the hardest as well as cherish the sweetest moments in life. Thank you for supporting me and motivating me during the writing of this thesis!

Finally, my family and partner Daniil. Without my parents I would not be where I am. Thank you for giving me an opportunity and freedom to pursue my passion. And thank you, Daniil, for always being there ready to listen and showing so much interest in my work.

List of publications

List of appended papers and author contributions.

Paper 1: Merdymshaeva, E., Mora, S., Machida, Y., Zhang, F., Duarte, F., Paul, S., Ratti, C., Mörtberg, U., 2025. *Assessing the impact of greenery on urban heat using opportunistic drive-by sensing*. *Environment and Planning B: Urban Analytics and City Science* 52: 1974–1993.

As the first author, EM took a major role in conceptualisation and design of the methodology, method development, investigation, software application, analysis and validation, writing and editing, and visualisation.

Paper 2: Merdymshaeva, E., Ghani, S., Lindberg, F., Simone, M., Dubey, R., Ljungqvist, L., Håkansson, A., Mörtberg, U., 2026. *Analysing the effect of tree canopy and urban form on urban surface heat using machine learning*. *Computers, Environment and Urban Systems*: (in prep).

EM is the first author of this paper and took a major role in conceptualisation, method development, investigation, software application and programming, analysis and validation, writing and editing, and visualisation. The paper is to be submitted.

List of abbreviations

AI	Artificial Intelligence
CI	Clearness Index
DEM	Digital Elevation Model
DS	Drive-by sensing
GNSS	Global Navigation Satellite Systems
GVF	Green View Factor
IR	Infrared
MAE	Mean absolute error
ML	Machine Learning
MSE	Mean squared error
RMSE	Root mean square error
RS	Remote Sensing
SD	Standard deviation
SEH	Sun-exposure heat
SHAP	SHapley Additive exPlanations
SUHI	Surface Urban Heat Island
SVF	Sky View Factor
T _{air}	Air temperature
T _{ambient}	Ambient temperature
T _{surf}	Surface temperature
UHI	Urban Heat Island
WS	Weather station

CONTENTS

1	Introduction	3
1.1	Surface temperature and air temperature.....	5
1.2	Measuring urban heat.....	6
1.3	Machine learning for spatial analyses	7
1.4	Research gap	8
1.5	Aim	9
2	Methodology	10
2.1	Study area	10
2.2	Data.....	11
2.2.1	Data captured with DS platforms.....	11
2.2.2	Other data sources.....	12
2.3	Methods.....	13
2.3.1	Pre-processing of DS data.....	13
2.3.2	Sample spots	14
2.3.3	Interpolations.....	14
2.3.4	Dependent variables	15
2.3.5	Independent variables	16
2.3.6	Statistical analyses	18
2.3.7	Machine learning for spatial data	18
3	Results.....	20
3.1	Paper 1.....	20
3.1.1	Comparisons with other data sources	21
3.1.2	Influence of greenery and grey structures on urban heat	23
3.2	Paper 2.....	26
3.2.1	Comparison between XGBoost and GPBoost for the sample spots	26
3.2.2	Analysing sample spots with GPBoost	28
3.2.3	Analysing observation points with GPBoost.....	30
3.2.4	Comparing models with and without tree shadows	32
4	Discussion	35
4.1	Comparisons of temperature data sources.....	35
4.2	Hot and cool zones related to greenery and grey structures.....	36
4.3	The DS approach for analysing UHI related to greenery	37
4.4	Applying machine learning to spatial data	37
5	Conclusions	38
	References.....	40

1 Introduction

Anthropogenic contributions to climate change in recent decades have triggered an unprecedented environmental crisis and led to the rise of multiple threats to whole ecosystems worldwide. For several reasons, urban environments are among the most exposed to increasingly severe weather patterns, including intensified heatwaves and prolonged droughts. Besides becoming more extreme, these events have also been observed to occur more frequently. As global urbanisation continues, cities are becoming both major contributors to climate change and particularly vulnerable to its impacts. One of the most widely recognised climate-related challenges affecting cities is the urban heat island (UHI) effect, which refers to the phenomenon where urban areas experience higher air and surface temperatures than surrounding rural environments (Oke et al. 2017; Santamouris 2018; Tuholske et al. 2021). The UHI effect is driven primarily by the replacement of natural land cover with artificial surfaces such as asphalt, concrete, and buildings, which modify the surface energy balance and microclimatic processes of urban environments (Oke et al. 2017; Roth 2013; Santamouris et al. 2019). These impervious surfaces typically have low albedo and high heat capacity, enabling them to absorb, store, and re-radiate solar energy at a higher rate than vegetated surfaces, thereby contributing to elevated temperatures in cities over longer periods.

The consequences of the UHI effect have significant implications for public health, energy consumption, and urban sustainability. Increased temperatures in cities have been linked to: spikes in energy consumption due to higher cooling demands (Santamouris et al. 2015); elevated health risks (Hao et al. 2025; Milojevic et al. 2016); and broader socio-economic impacts for urban environments (Oke et al. 2017; Santamouris 2018). In particular, prolonged exposure to extreme heat has been associated with increased mortality and morbidity, especially among vulnerable populations (Clarke 1972; Obradovich et al. 2017; van Someren 2003). Urban heat is therefore widely recognised as a major sustainability challenge affecting both environmental quality and human well-being (Tuholske et al. 2021). These impacts are relevant across different climatic contexts worldwide, including Nordic cities, where urban densification and rapid expansion may amplify heat-related risks despite relatively moderate regional climates compared to other parts of the world.

Urban areas can experience temperatures several degrees Celsius higher than those in surrounding rural areas due to the combined effects of urban materials, urban morphology, and anthropogenic heat emissions. Urban form, defined by the spatial configuration of buildings, streets, as well as green and open spaces, plays a key role in determining the microclimatic characteristics of cities. Urban geometry influences solar radiation exposure, potential heat storage, and wind circulation patterns, which together shape the spatial distribution of heat across urban landscapes (Depecker et al. 2001; Santamouris et al. 2019; Yang and Li 2015). This would include the sky view factor (SVF), defined as the fraction of visible sky from ground level, which has been shown to influence heat accumulation and dissipation processes (Theeuwes et al. 2017). Direct solar exposure can cause substantial increases in surface temperatures, depending on urban morphology and orientation (Dorman et al. 2019; Lindberg and Grimmond 2011).

At the same time, urban vegetation is of high significance for mitigating urban heat through shading, evapotranspiration, and modification of aerodynamic surface roughness (Venter et al. 2021). Green infrastructure, including green walls and roofs, street trees, parks, and urban forests, has been widely recognised as providing important ecosystem services that contribute to climate regulation and support human well-being (Burkhard et al. 2012; Keeler et al. 2019; Keesstra et al. 2018; Maes and Jacobs 2017). Several empirical studies have demonstrated significant cooling effects associated with urban greenery (Greene and Millward 2017; Gunawardena et al. 2017; Kraemer and Kabisch 2022; Quaranta et al. 2021; Venter et al. 2021; Venter et al. 2020; Wong et al. 2021; Zhao et al. 2020; Ziter et al. 2019). In these studies, tree canopy, in particular, was shown to reduce local temperatures by several degrees Celsius compared with areas dominated by impervious surfaces. According to some studies, tree cover and other urban green areas can even have a cooling effect on larger scales in the urban landscape (Branny et al. 2025; Zardo et al. 2017). In addition, water bodies may also influence local heat dynamics (Gunawardena et al. 2017; Kirschner et al. 2024).

The combined influence of grey and green urban structures on heat distribution highlights the importance of understanding the interplay between land cover, urban morphology, and microclimate processes. If extreme heat events are to be prevented or mitigated, it is essential to develop effective climate adaptation strategies and integrate the required measures into urban planning processes, thereby supporting sustainable and liveable cities (Visintin et al. 2025).

1.1 Surface temperature and air temperature

Urban heat island effects can be analysed using both air temperature (T_{air}) and surface temperature (T_{surf}), which represent related but distinct aspects of urban climate dynamics (Voogt and Oke 2003). Surface temperatures generally follow patterns similar to air temperature; however, their intensity and temporal dynamics may differ substantially, which is especially evident when comparing daytime and nighttime conditions (Roth et al. 1989; Shen et al. 2024; Zhang et al. 2014). Surface temperature is strongly influenced by the thermal properties of the immediate surroundings, including materials, albedo, heat capacity, and emissivity, which determine how surfaces absorb and release solar radiation (Mirzaei and Haghighat 2010; Oke et al. 2017; Venter et al. 2021).

Moreover, the intensity of surface temperatures is particularly dependent on hyperlocal characteristics such as urban morphology, land use, and SVF (Bärring et al. 1985; Zhao et al. 2025). In contrast, air temperature patterns are more affected by atmospheric conditions, including wind speed and direction (Azevedo et al. 2016). Several studies have shown that the intensity of surface urban heat island, also known as surface urban heat island (SUHI), typically peaks during daytime, when solar radiation directly heats surfaces, whereas air temperature UHI often peaks at night due to delayed release of stored heat from urban materials (Azevedo et al. 2016; Shen et al. 2024; Zhang et al. 2014).

Night-time heat retention has been linked to increased health risks because elevated temperatures during the night can lead to an extended exposure to heat, and limit physiological ability to recover from daytime heat exposure (Clarke 1972; He et al. 2022; Obradovich et al. 2017; van Someren 2003). Many health-related studies quantify heat exposure using daily mean air temperature exclusively (Lüthi et al. 2023). This highlights the importance of improving understanding of the relationships between T_{air} and T_{surf} , their variation across spatial and temporal scales, and their relation to health risks.

To summarise, surface temperature can be interpreted as the aggregated thermal response of individual urban elements, reflecting thermodynamic properties such as evaporation potential, surface roughness, and heat storage capacity (Mirzaei and Haghighat 2010; Oke et al. 2017; Venter et al. 2021). Because surface temperatures are strongly influenced by immediate environmental conditions, they provide important information about the thermal characteristics of urban land cover and their contribution to the UHI effect.

1.2 Measuring urban heat

UHI research relies on a range of measurement approaches; each associated with specific advantages and limitations. Traditionally, to quantify urban temperatures, ground-based weather stations were used, which typically provide air temperature observations with high temporal resolution and reliable measurements. However, this method has been noted to lack sufficient spatial coverage to capture microclimatic variability across heterogeneous urban landscapes (Sheng et al. 2017). As a result, weather station data may not adequately represent hyper-local variations in heat exposure at street level.

Remote sensing (RS) techniques provide an alternative approach by measuring land surface temperature (LST) using thermal infrared (IR) sensors mounted on satellites (Kim and Brown 2021b; Li and Schmidt 2024; Mirzaei 2015). Satellite-based measurements enable consistent and repeated observations across large geographic areas, thus supporting analysis of spatial patterns of urban heat (Streutker 2002; Tan et al. 2017). Common satellite platforms used for UHI research include Landsat 8, MODIS, and Sentinel-3, which differ in spatial resolution and temporal frequency (ESA 2022; NASA 2022; USGS 2023). Landsat 8 provides thermal imagery at approximately 100 m spatial resolution with a revisit time of 16 days, whereas MODIS and Sentinel-3 provide coarser spatial resolution but higher temporal frequency.

Despite their advantages, RS approaches have limitations related to spatial resolution, temporal resolution, and sensitivity to atmospheric conditions such as cloud cover (Hu et al. 2016). In addition, satellite measurements capture temperature from a nadir perspective, which limits the ability to capture vertical surfaces such as building facades and other areas beneath vegetation canopy (Arnfield 2003). The urban canopy layer, extending from ground level to the height of buildings and tree crowns, is considered particularly relevant for human thermal exposure and well-being (Oke 1976, 2004).

Several studies have attempted to overcome limitations associated with individual data sources by combining ground-based measurements with remote sensing observations (Schwarz et al. 2012; Sheng et al. 2017; Tan et al. 2017). However, the relationship between Tair and LST remains complex and not fully understood (Bechtel et al. 2017; Venter et al. 2021). Recent developments in data collection include the use of crowd-sourced weather stations (Chapman et al. 2017; Venter et al. 2021) and mobile sensing approaches such as bicycle-based measurements (Ziter et al. 2019) and

unmanned aerial vehicles (Rodríguez et al. 2022; Song and Park 2020; Zhao et al. 2020). While some of these approaches focus primarily on measuring air temperature, others measure surface temperature but are often limited in spatial coverage.

Drive-by sensing (DS) has emerged as a promising technique for capturing environmental data across urban landscapes (Cummings et al. 2021; de Souza et al. 2020; Zhao et al. 2021). DS approaches typically involve equipping vehicles with sensors that collect measurements as they move through urban areas. This enables extensive spatial coverage and high-resolution data collection (both spatial and temporal) at relatively low cost. In the first study, a DS platform, City Scanner, was deployed as an opportunistic environmental sensing system capable of capturing air and surface temperature data across the urban environment (Paper 1). The platform was mounted on three-wheeled electric taxi vehicles that could cover vast areas of the inner city of Stockholm. For the second study, the next iteration of the platform, Flatburn, was used on the same vehicles over the whole summer of 2022 (Paper 2).

These studies examined the serviceability of opportunistic drive-by sensors for capturing hyperlocal variations in surface temperature. In this study, City Scanner sensors mounted on electric vehicles enabled the collection of high-resolution thermal data at street level, providing detailed information on the spatial and temporal variability of urban heat patterns. This approach allows direct observation of temperature variation within the urban canopy layer and enables improved analysis of relationships between urban structure, vegetation, and microclimate.

1.3 Machine learning for spatial analyses

Advances in data availability and computational capacity have enabled the application of machine learning (ML) methods to analyse complex spatio-temporal relationships between urban form and heat patterns. Traditional spatial statistical approaches can capture spatial relationships, spatial autocorrelation and certain temporal patterns in environmental data, but they often assume linear relationships between variables. This can be considered as an important limitation, as urban heat dynamics are simultaneously influenced by multiple interacting variables that may exhibit non-linear relationships, thus making the results of linear statistical models potentially biased or incomplete.

In contrast, ML approaches provide greater flexibility for modelling complex, non-linear relationships in spatial data. Tree-based methods such as Random

Forest and Gradient Boosting have increasingly been applied in environmental modelling due to their ability to capture interactions among variables without requiring strict assumptions regarding data distribution. Moreover, among boosting-based algorithms, XGBoost has demonstrated strong performance compared to both statistical models and Random Forest approaches in terms of prediction accuracy, runtime, and computational efficiency (Li 2022; Wu et al. 2023).

Nevertheless, conventional ML models may not explicitly account for spatial and temporal dependencies inherent in environmental data. To address these limitations, hybrid modelling approaches combining statistical spatial components with boosting algorithms have been proposed, including models such as GWRBoost and GPBoost (Sigrist 2021; Wang et al. 2026). These approaches aim to incorporate the strengths of machine learning with spatial statistical modelling to better represent spatial heterogeneity and non-stationarity in environmental processes.

The integration of ML with high-resolution environmental sensing data provides new opportunities to analyse complex interactions between urban morphology, greenery, and surface temperature. Therefore, by combining opportunistic IR measurements with ML algorithms, it becomes possible to analyse large and complex spatial datasets that capture hyperlocal variation in urban heat patterns.

1.4 Research gap

Despite extensive research on UHIs, important knowledge gaps remain regarding the spatial distribution and effectiveness of urban greenery in mitigating heat at hyperlocal scales. While previous studies have demonstrated the cooling potential of vegetation, there remains a limited understanding of how interactions among urban form, tree canopy, and microclimate vary across detailed spatial scales within cities.

Existing temperature datasets often lack sufficient spatial and temporal resolution to capture fine-scale variability in urban heat patterns. RS data provide broad spatial coverage but may not adequately capture microclimatic conditions within the urban canopy layer. Ground-based weather stations provide high temporal resolution but limited spatial representation. Emerging data collection methods such as drive-by sensing offer new opportunities to capture hyperlocal environmental data across urban landscapes.

There is increasing interest in combining opportunistic sensing approaches with ML techniques to deepen understanding of urban surface heat patterns

and their relationship to urban morphology and vegetation. Leveraging high-resolution IR surface temperature measurements and analysing them using ML algorithms bring prospects for the development of more accurate and spatially detailed models of urban heat distribution.

Such approaches can provide new insights into the relationships between grey and green urban structures and their influence on street-level thermal conditions. Improved understanding of these relationships may support the development of evidence-based urban planning strategies to mitigate heat exposure and enhance climate resilience in cities.

1.5 Aim

The overall aim of this study is to explore a novel methodological approach for capturing and analysing urban heat data with high spatial and temporal resolution across the urban landscape. The study investigates relationships between urban form, tree canopy, and surface temperature using opportunistic environmental sensors and advanced ML techniques.

Specifically, the study aims to develop and evaluate a DS platform capable of collecting high-resolution air temperature and surface temperature data across the inner city of Stockholm, Sweden. The study further aims to compare opportunistically collected temperature data with other data sources and to develop models capable of analysing relationships between surface temperature, greenery, and grey urban structures at hyperlocal scale.

The specific targets were to: 1) explore the differences in temporal and spatial patterns of urban heat as observed by drive-by sensing, compared to other data sources; 2) estimate the impact of greenery in combination with grey structures on urban heat island effects at street-level scale, using ML techniques; and 3) explore the use of this opportunistic high-resolution data in models explaining urban heat with independent variables on different scales, from hyperlocal to landscape, to support improved analysis of urban heat island problems.

By addressing these questions, the study contributes to methodological development in urban climate research by integrating opportunistic IR sensing with ML techniques to analyse urban heat patterns at high resolution. This approach provides an opportunity to improve understanding of interactions between urban morphology, vegetation, and thermal conditions within the urban canopy layer. Improved knowledge of these relationships can support urban planning and climate adaptation strategies that promote safe, sustainable, and liveable urban environments.

2 Methodology

2.1 Study area

Both Paper 1 and Paper 2 focused on the City of Stockholm, the capital of Sweden. Stockholm is located at 59N 18E (WGS-84), spanning over 188 km² with approximately 989000 inhabitants. The municipality consists of several land cover types, where 33.8% forest and other tree cover, 12.7% water bodies, 21.8% open land and 31.7% built environment (SEPA 2018). The area covered by DS platforms is predominantly in the city centre. A combined study area including both 2021 and 2022 is shown in Figure 1.



Figure 11. Combined study areas that include both 2021 and 2022 studies.

2.2 Data

2.2.1 Data captured with DS platforms

During both the 2021 and 2022 studies (Paper 1 and Paper 2) surface heat, alongside other variables, was captured with DS platforms developed by MIT (<https://senseable.mit.edu/cityscanner>, <https://senseable.mit.edu/flatburn/>). This approach enabled getting high spatial and temporal resolution data covering large parts of the inner city of Stockholm, as shown in Figure 1. In both case studies the platforms were deployed on roofs of 3-wheeled electric vehicles driving on demand; the platforms were placed at 1.5 m height. These electric vehicles were used as taxis in 2021 and later transitioned to delivery service in 2022. However, this did not have a significant impact on the data, as the vehicles' operational area remained the City of Stockholm. Because the vehicles are classified as mopeds, their speed is restricted to 45 km/h.

The DS platform is solar-powered and self-contained, so it typically does not require additional maintenance once deployed. For data retrieval and maintenance, the platform can be accessed via the cellular network. To save energy and avoid redundant data storage, the platform does not continuously measure. Instead, it relies on an accelerometer to detect movement and only then activates other sensors. However, vehicles were parked in a garage indoors, which was also situated below ground level with no large windows. This in turn led to the platform being taken down for charging and data download occasionally.

It was not only the company that went through changes between 2021 and 2022 – in the second run a new version of scanner was used. The 2021 version is called City Scanner (<https://senseable.mit.edu/cityscanner>), whilst the later iteration is Flatburn (<https://senseable.mit.edu/flatburn/>). The City Scanner utilised a single-pixel IR sensor for measuring surface heat, and an air temperature sensor. The field of view of the IR sensor was 70 degrees vertically and 120 degrees horizontally, and the measured output surface temperature (Tsurf) was the average of all objects within the field of view. The IR sensor was placed perpendicularly and facing to the right, at a 90-degree angle to the vehicle's driving direction, which meant it faced facades and other objects while outside. Apart from Tsurf and Tair, parameters in the output dataset included: device ID; timestamp in UNIX format; Tambient (ambient surface temperature used for control); and GNSS coordinates in WGS-84. The recordings were made with a predefined 5-second interval. With 5 deployed vehicles and a data-collection period from July 26th to August 31st of 2021, around 520 thousand data points were collected.

As mentioned before, a different version of the DS platform was used during the summer of 2022. While most of the components were similar, two major changes were made for the second case study. Firstly, a higher resolution IR sensor was implemented: instead of a 1-pixel output, the recorded data was 32x24 pixels. This allowed for a more detailed analysis of surface heat as well as detection and handling of the possible edge effects. Secondly, instead of a perpendicular alignment, the IR sensor was tilted 5° downward to capture more of the ground, to better understand relationships between ground and façade surfaces, and to avoid capturing data from a long distance. In 2022, the data collection period ran from the 20th of May to the 31st of August, covering the entire summer. With 5 deployed scanners, this resulted in over 500 thousand data points recorded.

2.2.2 Other data sources

The variables and data sources vary between Paper 1 and Paper 2. An overview of all the data used in both papers is presented in Table 1.

Data	Paper	Source
Data on air temperature, humidity, and global radiation from ground-based weather stations	P2	SLB-analys (2024)
Google street-view images 2009-2012, 2014 and 2016-2021	P1	Google (2022)
National road database (Nationella vägdatan, NVDB, Transportstyrelsen)	P1 and P2	Swedish Transport Agency (STA 2021)
Digital elevation model, 2x2 m	P1 and P2	Lantmäteriet (2022)
Building footprints and heights	P1 and P2	City of Stockholm (2019)
Building footprints outside the borders of the City of Stockholm, from the Property Map	P1 and P2	Lantmäteriet (2023)
Water bodies from the Property Map	P1 and P2	Lantmäteriet (2023)
Tree canopy data	P1 and P2	City of Stockholm (2020)
Tree canopy data from Google Environmental Insights Explorer (EIE) data	P2	Google (2024)
Tree canopy data, including tree heights	P2	Boverket (2023)
Satellite imagery	P1	Landsat (Earth Resources and Science 2020)

2.3 Methods

2.3.1 Pre-processing of DS data

To prepare the collected data for analysis, several steps were taken in both Paper 1 and Paper 2. In Paper 1, the data were “split” into two subsets:

- all active hours of the DS platform;
- night and morning time slice, where only data from 0 to 10 am were picked. This subset was created to analyse the surface capacity for heat relief separately, which is vital for human health.

Moreover, only measurements with an estimated vehicle speed between 5 and 65 km/h were selected. This was done to avoid oversampling and to avoid possible effects from heat emitted by other surfaces (e.g. vehicle roofs) that were more prominent in a standing or low-speed mode. The lower value was chosen because the air temperature sensor on the DS platform requires airflow for more accurate readings. Then, a visual inspection of the measurements was made, and unrealistic observations were removed. Lastly, all faulty records, i.e. records with extreme outlier values, and missing data were removed before the analyses.

In Paper 2, a similar approach was followed, though with several deviations. To analyse the development of the difference between surface heat and air temperature, the dataset was split into three subsets:

- morning (8.00-10.00)
- afternoon (14.00-16.0)
- evening (20.00-22.00)

As in the previous case study, data with extreme or missing values were removed. However, since Flatburn used a 32x24 pixel resolution IR-scanner, resulting in 768 surface temperature values per one measurement, it was possible to remove specific outliers from a single set instead of withdrawing the whole record. Afterwards, the mean of the remaining values was calculated. As the next step, thresholds of 2 km/h and 65 km/h were used to avoid oversampling. The lower interval value differed in Paper 2 because the analyses and modelling did not involve air temperature measured by the DS platform. This was followed by a visual inspection of the remaining datapoints.

Lastly, for Paper 1, the remaining points were filtered based on measurement density. Therefore, to avoid under-sampling, we tested using only sample spots with at least 128 measurements throughout the study period (36 days).

Furthermore, in Paper 2, the 2022 data points were map-matched, meaning

that, with the help of an open-source algorithm called Valhalla Meili, new coordinates were calculated. These new coordinates were set to follow the road network of Stockholm, resulting in the points being moved to the probabilistically most likely roads the DS platform had been driving on. Then, using a bearing angle between consecutive points, the third set of coordinates was calculated, with the output points placed geodetically 5 m to the right (90°) of the direction of movement (Merdymshaeva 2026). In this way, some errors in global positioning could be minimised, and data from vehicles driving in different directions on a street could be properly separated.

2.3.2 Sample spots

For planning-relevant analyses at the local level, to reduce temporal effects, we aggregated the original datapoints into a different unit of assessment, called sample spots. Sample spots are circles with a diameter of 30m; they are created on each side of the road's centreline to capture effects specific to each roadside. This unit of assessment was used to sample surface heat interpolations, interpolated differences between surface and air temperatures, and local and focal values of the independent variables within specified ranges (Table 2).

An example of sample spots placed on top of a satellite image and then shown together with the interpolated difference between surface and air temperature can be seen in Figure 2.

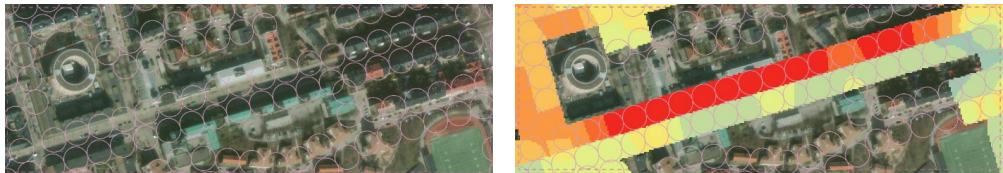


Figure 2. a) A snapshot of streets with sample spots on either side of the middle-of-the-road, and b) adding the road buffer separating the traffic lanes in different directions, with interpolation of ST. Red colours show hot ST, and green-blue shows cooler ST.

2.3.3 Interpolations

As mentioned, it is important to capture surface heat variations on each side of the road, as differences can be significant due to a number of local and hyper-local factors (such as sun exposure). To achieve that, two sets of buffers were created on the topological right and left sides of the line representing the middle of the road. The buffer width was set to 30 m to account for potential

GNSS positioning errors and uncertainties (for both Papers 1 and 2) and possible map-matching errors (Paper 2 only).

In the next step, surface temperature measurements (direct in case of Paper 1 and mean of all the scanned pixel values in Paper 2) and difference between surface and air temperature from weather stations (derived per hour) were interpolated separately within the matching buffer zone. The chosen interpolation technique was Diffusion within barriers, with 90 m and 30 m search in Paper 1 and 2, respectively. This method was preferred over others as it is using the Heat equation as its core. Since in some cases (e.g., crossroads, turns) the buffer zones might overlap, the average of both buffers was calculated when combining the two interpolated datasets.

2.3.4 Dependent variables

In Papers 1 and 2, two different approaches were taken to describe T_{surf} changes across the city of Stockholm. For Paper 1, a sun-exposure heat (SEH) index was used. Meanwhile, in Paper 2, the differences between the surface measurements and air temperature ($\Delta ST-AT$) represented the dependent variable.

2.3.4.1 Sun-exposure heat index

For the surfaces that were potentially visible by the DS platforms, an index incorporating radiant heat and sun-exposure hours was derived from the interpolated T_{surf} and average values of “visible” sunhours within the sample spots (Equation 1):

$$SEH = \frac{\text{radiant heat}}{\log(\text{sunexposure hours})} \quad \text{Equation 1}$$

The SEH index was estimated using samples of interpolated T_{surf} and mean values of sun-exposure hours per visible areas within the sample spots. In this way, the T_{surf} value would be balanced against the level of sun exposure in an area.

2.3.4.2 Difference between T_{surf} and T_{air}

Paper 2 focused on identifying areas with abnormal surface temperatures relative to a reference value, derived from the contemporary T_{air} value as measured by the stationary weather station. T_{surf} relies heavily on immediate land-use types, materials, and urban form, while T_{air} exhibits less fluctuation

within the same environment. In addition, all measurements were taken within the canopy layer of Stockholm, and only the city centre was analysed. Therefore, the difference between surface and air temperatures ($\Delta\text{ST-AT}$) was chosen as the dependent variable, allowing the identification of which parameters may have affected the temperature difference at a hyper-local scale.

2.3.5 Independent variables

While the analyses in Papers 1 and 2 shared the same idea, the exact variables, their resolutions, sources, and treatments differed. The independent variables used in both papers are listed in Table 2. The main idea for the analyses was to identify and quantify the impact of nature-based solutions, especially tree canopies combined with urban form, on different scales. In urban areas, the parameters that would affect $\Delta\text{ST-AT}$ were split into three main categories: urban form, greenery and water bodies.

Urban form included sun-exposure (hours), sky view factor (percentage of the overall urban canopy), building area and volume (share from each sampled area). Greenery was represented by the percentage of tree canopy in each sampled area. Water bodies followed the same logic as greenery, but with data on water-body area. The sampled areas were based on map-matched observation points with the $\Delta\text{ST-AT}$ values, and sample spots, following several scales: hyper-local (measurement scale, local and focal values from a single point), local (sample spot level, within a spot as well as focal statistics within 15-30 m), district (sample spots within 100-300 m focal area), and landscape (sample spots within 600-1000 m focal area).

The variable “sun-exposure” is the number of hours a unit of assessment has been exposed to the sun. This variable was intended to aid in the exploration of several parameters related to the urban canyon without having to include them separately, which is beneficial when some data are unavailable.

For the estimation of sun-exposure hours, the Daily Shadow Pattern tool from UMEP QGIS plugin was used (Lindberg et al. 2018). Its results were based on the input digital surface model (DSM), a sum of a Digital Elevation Model (DEM) (Lantmäteriet 2022) and building footprints and their respective heights (City of Stockholm 2019). Furthermore, for Paper 2, an additional version of the sun-exposure hours was calculated. This version included the tree canopy to identify the impact of tree shadows. Shadow patterns were estimated hourly throughout the study period (both Paper 1 and Paper 2).

The sun-exposure hours were then summed up over the whole study period to match each subset of modelled data (whole day and nighttime for Paper 1;

morning, afternoon and evening for Paper 2). Whilst Paper 1 focused more on the transition period between night and morning, Paper 2 prioritised afternoon data to analyse an expected peak in heat.

Since sun-exposure was estimated from a top-down view and surfaces measured by DS platforms would be limited by their field of view, it was important to exclude effects from surfaces that would not be visible to the IR-scanner traversing the streets. To do this, visibility analyses were performed using streets as observers, with the height set to 1.5 m, approximately where the scanners would be. Next, this was used as a “barrier” for sun-exposure data.

Sky view and green view factors (SVF and GVF), respectively, were retrieved from Google Street View images (© Google 2009-2019), with both used in Paper 1 and only SVF tested in Paper 2. This enabled us to further describe the qualities of urban canyons across Stockholm.

To capture more of the urban form, the direction of the sensors was estimated (i.e., the bearing angle from the North and 90° to the topological right of the vehicle's movement). This was used in Paper 2 on point data, alongside the timestamp, to achieve an even higher spatio-temporal resolution.

Furthermore, the collected data were compared with Landsat 8 satellite imagery. This was done to identify areas with significant differences between land surface temperatures from an up-top view and facade-ground surface temperatures inside the canopy layer (see Paper 1).

Table 2. Independent variables derived from different data and on different scales.

Independent variables	Based on data
Sun-exposure hours: shadows from terrain and buildings	DEM (Lantmäteriet 2022), Building polygons (City of Stockholm 2019)
Sun-exposure hours: shadows from terrain, buildings and trees	DEM (Lantmäteriet 2023), Building polygons (City of Stockholm 2019), DSM (from laser scanned datacloud, Lantmäteriet 2023)
Skyview factor	Google (2022)
Greenview factor	Google (2022)
Built-up area from local to landscape (within 15, 30, 100, 300 meters)	Building polygons (City of Stockholm 2019)
Built-up area on landscape scale (within 600 and 1000 meters)	Building polygons (Lantmäteriet 2023)
Building volume from local to landscape (within 15, 30, 100, 300 meters)	Building polygons with heights (City of Stockholm 2019)

Tree canopy from local to landscape (within 15, 30, 100, 300 meters)	Tree polygons (City of Stockholm 2020)
Tree canopy from local to landscape (within 15, 30, 100, 300 meters)	Google Environmental Insights Explorer (EIE) data (Google 2024)
Tree canopy from local to landscape (within 15, 30, 100, 300, 600, 1000 meters)	Boverket (2023)
Water from local to landscape (within 15, 30, 100, 300, 600, 1000 meters)	Water from the Property map (Lantmäteriet 2023)
Sensor direction	Direction of the IR-sensor, calculated using map-matched positions of the measurements
Timestamp	Timestamp from the DS platforms dataset, in UNIX format
Land surface temperature	Land surface temperature estimated from Landsat imagery (Paper 1)

2.3.6 Statistical analyses

In Paper 1, Pearson's correlation with a 95% confidence interval was used to analyse the relationships between the explanatory variables (green and grey structures) and the dependent variables (DS Tsurf and the SEH index). Both the values and their distributions were then compared. Moreover, multiple linear regression was applied to the same parameters to further understand the relationships (Krzywinski and Altman 2015).

In Paper 2, for a deeper investigation of the changes in the local impact of canopy share on the model output, ML output values from both models (with and without tree shadows included) and the variable itself (share of tree canopy within 15 m) were mapped. As the next step, Hot Spot Analysis (Getis-Ord G_i^*) was run for each parameter, followed by the Hot Spot Analysis Comparison.

2.3.7 Machine learning for spatial data

To explain Δ ST-AT ML Tree-Boosting algorithms were used, because they were proven to outperform classical geostatistical models when it came to modelling with a set of correlated variables (Li 2022), which is the case for urban form parameters in Paper 2. Despite the benefits, Tree-Boosting algorithms often underperform on tasks involving spatial parameters. Therefore, we decided to apply two models and compare their results: XGBoost and GPBoost. All modelling was performed using Python and relevant packages.

While XGBoost only works with Tree-Boosting, GPBoost is split into two parts: Gaussian process and Tree-Boosting. Consequently, the results of modelling

highly variable data with XGBoost can be unstable when coordinates are used in the model. To improve the output, the coordinates were used in their scaled form instead, i.e., as distances between the points. However, in the case of GPBoost, the Gaussian process is specifically designed to be used for random effects at observed locations, enabling it to handle spatio-temporal variables (Sigrist 2024).

For cross-validation, the data sample was divided into subsets for model training and testing, 80% and 20%, respectively. For the training dataset, Vecchia approximation and pre-fitting were used in GPBoost to speed up the models' respective runtimes. To compare XGBoost and GPBoost performance, several metrics were adopted: Root Mean Square Error (RMSE), Mean Square Error (MSE), Mean Absolute Error (MAE) and R-squared (R^2).

Furthermore, for analysis of the importance and impact of the independent variables, the following coefficients of their respective contributions were estimated: SHapley Additive exPlanations (SHAP), Gain and Split. The latter two are retrieved from the model results. Gain explains how much interpretability is essentially gained by the model using a specific variable. Split, on the other hand, is the number of times a variable is used to create a new "branch" of the tree-algorithm, i.e. the algorithm evaluates which variable to use for the next split in data in order to avoid information being lost (Zhang et al. 2022).

SHAP, a method originating from game theory, is nowadays applied in multiple AI models (Padarian et al. 2020). This tool can quantify the significance of the individual input of each variable, as well as establish their hierarchy. Another important benefit of this technique is that it can provide both global and local explanations, which is crucial for grasping the spatial processes in an urban environment (Elhishi et al. 2023).

3 Results

3.1 Paper 1

Data collected by the DS platforms (Tair, Tsurf and Tambient) are shown in Figure 3 alongside the data from WS – in 2021 there were four functional ones within the study area. All measurements are reported as hourly means to ensure they follow the same temporal distribution.

As shown in the figure, both datasets follow similar patterns. DS Tair and DS Tambient are strongly correlated, indicating a good performance of the IR sensor. Furthermore, DS Tair and DS Tsurf show a significant correlation as well, with the coefficient being 0.876, $R^2 = 0.767$, and $p < 0.001$. However, Tsurf values have higher maximum and minimum values, with plummets and ascents being more extreme: the difference between the two ranged from -15.2°C to 22.8°C , with a standard deviation of 2.5°C . On average, the difference between Tsurf and Tair from the DS platforms was 1.00°C .

All measurements were visualised in ArcGIS, following the preprocessing described earlier. When represented in a map (Figure 3), the data shows more information about the spatial distribution of DS Tsurf: while the dataset with all-hours has overall higher values, it is more evenly distributed; at the same time, the morning subset has more distinct zones with extreme hot and cold zones. In 2021, data from the whole study period were analysed together, meaning that these patterns are generalised and can provide interesting insights into the local urban climate.

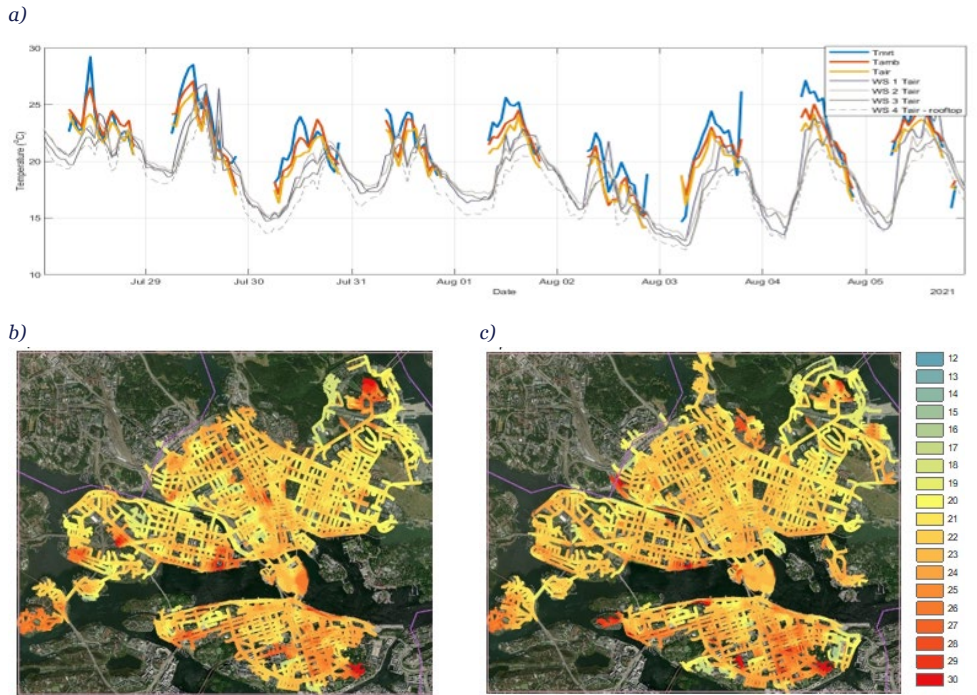


Figure 3. Outcomes of the heat measurements from the DS platforms and comparisons with the stationary WSs. In a) a snapshot between 28th of July and 6th of August 2021, hourly mean values of the measurements for both data sources. The DS platforms measure T_{surf} and T_{amb} (measured with an IR device), and T_{air} , while the four WSs measure T_{air} . In b) DS T_{surf} during night-and-morning hours, and c) DS T_{surf} for all hours during the day.

3.1.1 Comparisons with other data sources

From the differences between DS T_{surf} and WS T_{air} from the morning and all-hour periods, it can be observed that the morning surface temperatures were marginally warmer than the corresponding air temperatures. This indicates that surfaces store and emit heat overnight. At the same time, several zones had colder surface temperatures in the all-hour subset. Moreover, there are fewer areas with extremely high temperature differences, with the overall pattern being more levelled. These patterns are illustrated in Figure 4.

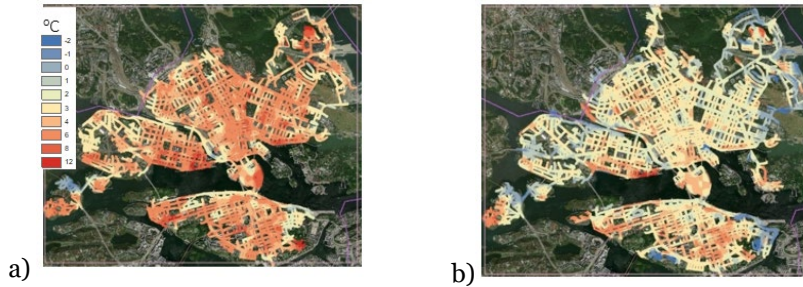


Figure 4. Map a) shows the difference between DS Tsurf and the WS Tair, for night-and-morning hours (0-10 am) for the sample spots during the summer 2021. Map b) shows the difference between DS Tsurf and the WS Tair, for all hours recorded for the sample spots during the summer 2021.

To identify differences between surface temperatures derived from RS top-down and DS to-the-side methods, DS Tsurf was then compared to RS LST. Only measurements from the same time periods were selected from both datasets. These were matched spatio-temporally in order to achieve a better understanding of local effects.

DS Tsurf values from the compared values ranged between 19.8°C and 36.4°C, with the mean value of 25.0°C and SD \pm 3.32 °C. At the same time, RS LST values ranged between 16.9 and 23.9°C, with the mean being 21.7 °C and SD \pm 1.71 °C. This means that on average DS Tsurf was 3.3 °C higher. These datasets were strongly correlated ($R = 0.244$, $R^2 = 0.060$, $p < 0.001$, $N=186$), the results are shown in Figure 5.

Furthermore, eight outliers were identified (a) in Figure 5. Upon visual inspection, it was revealed that they were located close to each other. Moreover, all these outliers were from measurements of facades facing South and South-South-East. These facade temperatures were higher than the road temperatures, which would be a result of the strong sun exposure during that time of day.

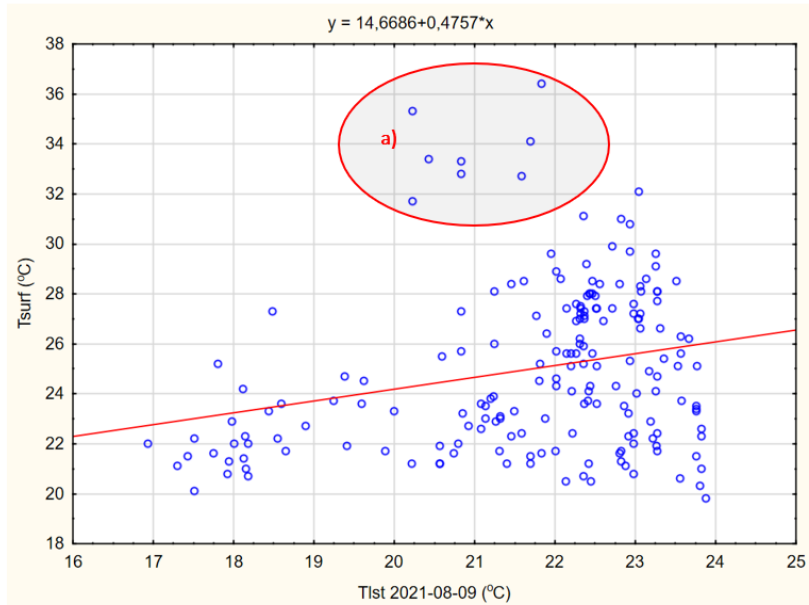


Figure 5. Comparison between LST and Tsurf, using the cloud-free zone of the central study area that was available during the 36 monitored days, i.e. 9 August 2021 (n = 186). The encircled outlying values (a) were selected for visual inspection.

3.1.2 Influence of greenery and grey structures on urban heat

Two predictive multiple regression models were used to quantify and further analyse the impacts of different parameters on the distribution of surface heat and its patterns. In this case study, urban form was represented by SVF, since it can describe the amount of open sky, and thus the density of buildings and other high structures in the area, including tree canopy. This variable was complemented by GVF, which represented all visible greenery: it would capture evapotranspiration from all types of green cover, as well as potential shading from tree canopies. With the latter, the larger the canopy, the larger the shadow it casts. In addition, in several tests, the SEH index was used as a dependent variable to balance Tsurf with sun exposure hours. Correlations between DS Tsurf and both SVF and GVF, as well as the relation between SEH index, SVF and GVF, are shown in Figure 6.

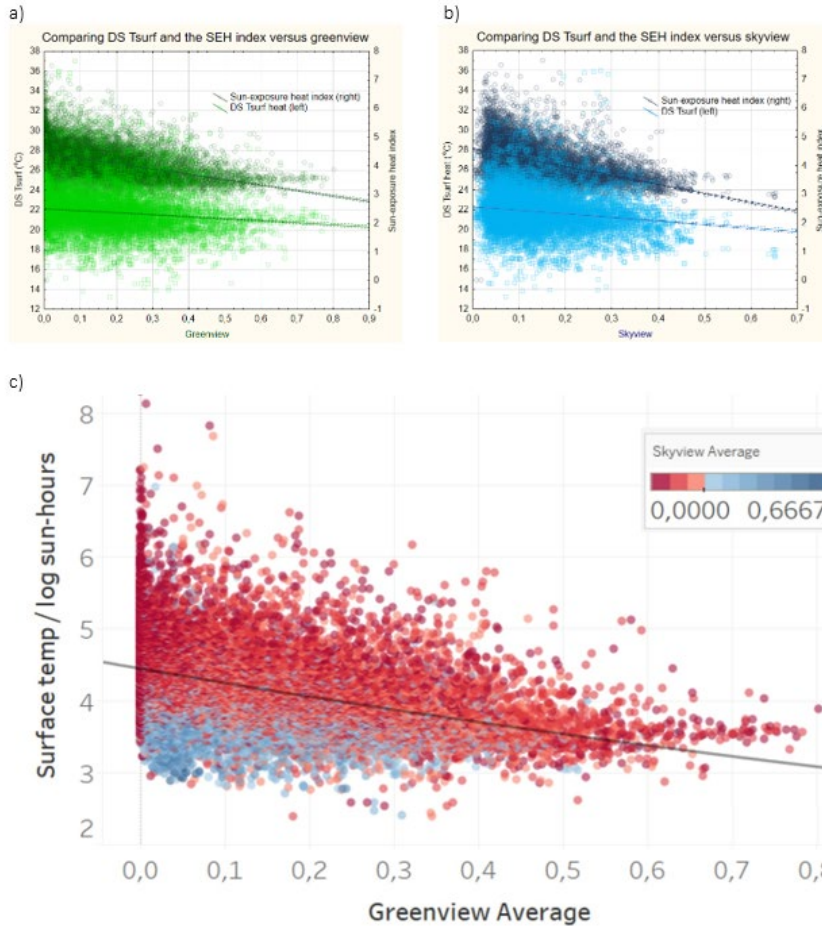


Figure 6. Comparison between DS Tsurf and the SEH index for all sample spots, versus: a) GVF influence on DS Tsurf and the SEH index, b) SVF influence on DS Tsurf and the SEH index, and c) GVF influence on DS Tsurf in combination with illustrating sample spots with high SVF in blue.

From Figure 6, it is evident that the SVF was negatively correlated to both DS Tsurf ($R = -0.174$, $R^2 = 0.030$, and $p < 0.001$) and the SEH index ($R = -0.476$, $R^2 = 0.226$, and $p < 0.001$). This shows that more open areas tend to be cooler. As for the GVF, it is also negatively correlated with the modelled variables: DS Tsurf ($R = -0.150$, $R^2 = 0.022$, and $p < 0.001$) and the SEH index ($R = -0.434$, $R^2 = 0.189$, and $p < 0.001$).

Since SVF is also dependent on the amount of tree canopy, meaning higher SVF could be a result of lower GVF, it was vital to analyse their impact together in a model. Multiple regression results show that the SEH index performed better than DS Tsurf when SVF and GVF were included as predictors. For DS Tsurf the results were: $R = 0.225$ and $R^2 = 0.050$, and $p < 0.001$. For the SEH index, the results were: $R = 0.631$, $R^2 = 0.398$, and $p < 0.001$. As expected, it can be concluded that including sun exposure in the analyses can significantly improve the results (Figure 6c).

Due to the opportunistic nature of the data from the DS platforms, the relations were tested on a subset, with sample spots containing at least 128 measurements across the entire study period (36 days). This test showed stronger correlations between dependent and independent variables. For SVF: DS Tsurf ($R = -0.212$, $R^2 = 0.045$, $p < 0.001$), and the SEH index ($R = -0.543$, $R^2 = 0.294$, $p < 0.001$). For GVF: DS Tsurf (-0.400 , $R^2 = 0.160$, $p < 0.001$), and the SEH index ($R = -0.583$, $R^2 = 0.340$, $p < 0.001$). Modelling was then performed again for this new subset, showing even better results: DS Tsurf predicted by GVF and SVF (Multiple $R = 0.394$, $R^2 = 0.155$, $p < 0.001$), and the SEH index predicted by the same variables (Multiple $R = 0.703$, $R^2 = 0.494$, $p < 0.001$). More information on all models is available in Table 3.

Table 3. Results from analyses of sample spots with different minimum numbers of observations.

Sample 1 (spots with >8 samples)						
N=13967	Dependent variable: SEH-index					
	R= 0,63079927 R ² = 0,39790771 Adjusted R ² = 0,39782148					
	F(2,13964)=4614,2 p<0,0000 Std.Error of estimate: 0,47525					
		b*	Std.Err.	b	Std.Err.	t(13964)
Intercept			4,86024	0,008332	583,3447	0,00000
skyview_average	-0,457804	0,006573	-3,01693	0,043314	-69,6531	0,00000
greenview_average	-0,414478	0,006573	-1,79407	0,028450	-63,0613	0,00000

Sample 2 (spots with >128 samples)						
N=2314	Dependent variable: SEH-index					
	R= 0,70318397 R ² = 0,49446770 Adjusted R ² = 0,49403020					
	F(2,2311)=1130,2 p<0,0000 Std.Error of estimate: 0,37272					
		b*	Std.Err.	b	Std.Err.	t(2311)
Intercept			4,92747	0,016263	302,9776	0,00000
skyview_average	-0,501083	0,014925	-3,25053	0,096819	-33,5732	0,00000
greenview_average	-0,430688	0,014925	-2,17765	0,075464	-28,8567	0,00000

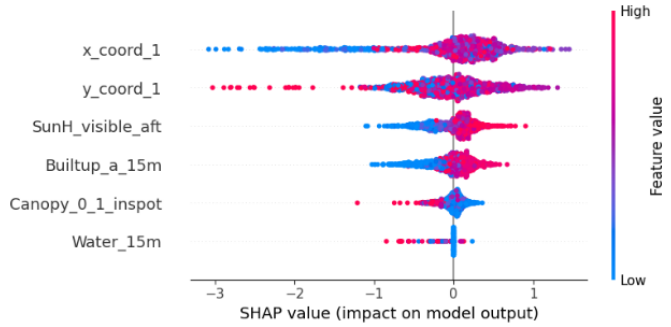
3.2 Paper 2

After preprocessing, 218,603 data points remained. Then, data were selected for modelling only those from the afternoon and only those with a Clearness Index (CI) higher than the median of 0.66; a total of 16,094 data points remained. As for the aggregated data, 6675 sample spots in total were analysed, including only afternoon values with the same CI threshold.

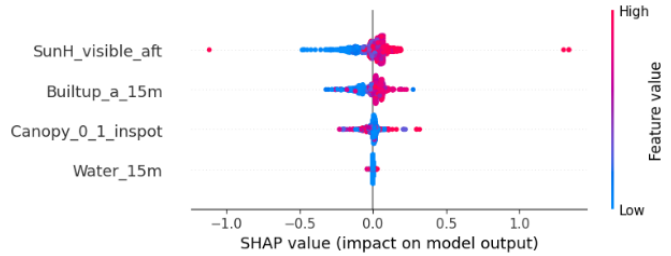
3.2.1 *Comparison between XGBoost and GPBoost for the sample spots*

To compare model performances, both XGBoost and GPBoost were tested with the same set of explanatory variables. The variables are presented in Table 2 along with their respective descriptions. The models were run for the sample spots, applying different radii (spatial resolutions) for data aggregation, so that temporal parameters could be omitted. As a result, the hyperlocal scale with immediate local parameters had the highest explanatory power. Overall, GPBoost outperformed XGBoost, with average R^2 (separately comparing the different radii) of 0.85 and 0.60, respectively. RMSE and MAE were higher with XGBoost, indicating that the evaluated model errors were lower with GPBoost, further underscoring its better performance. The difference is most likely due to the high spatial variation in Tsurf, where GPBoost is expected to outperform XGBoost. This could be explained by GPBoost separately handling spatial parameters (coordinates) within the Gaussian process part. All results, model performance analysis, and SHAP values are presented in Figure 7.

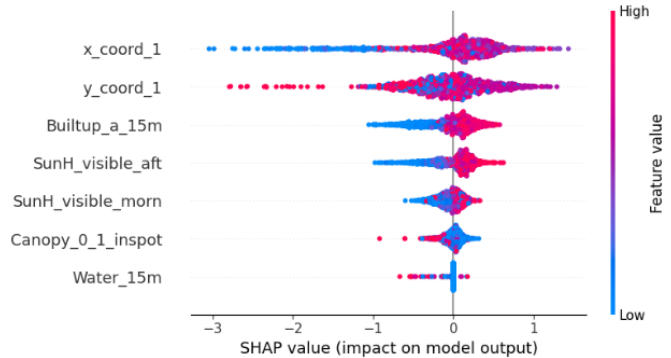
Model a) XGBoost: coordinate distances, canopy (Boverket) inspot, sun-hours afternoon, builtup area within 15 m, water within 15 m
 $R^2 = 0,595$; RMSE = 0,968; MAE = 0,708



Model a) GPBoost: canopy (Boverket) inspot, sun-hours afternoon, builtup area within 15 m, water within 15 m
 $R^2 = 0,852$; RMSE = 0,594; MAE = 0,347



Model b) XGBoost: coordinate distances, canopy (Boverket) inspot, sun-hours afternoon, builtup area within 15 m, sun-hours morning, water within 15 m
 $R^2 = 0,603$; RMSE = 0,950; MAE = 0,698



Model b) GPBoost: canopy (Boverket) inspot, sun-hours afternoon, builtup area within 15 m, sun-hours morning, water within 15 m
 $R^2 = 0,857$; RMSE = 0,585; MAE = 0,339

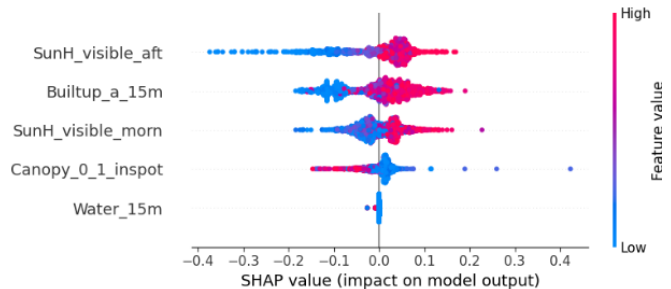


Figure 7. Parameters, model and feature importance of the two best models to explain surface heat differences ($\Delta ST-AT$), comparing XGBoost and GPBoost

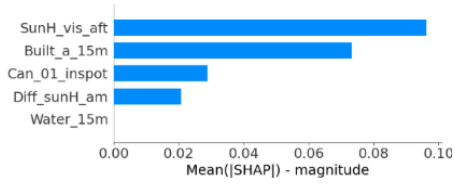
3.2.2 Analysing sample spots with GPBoost

During GPBoost tests, the variables' impact on the model (SHAP, Gain and Split values) was plotted to better understand their importance for the output. These plots are shown in Figure 8. From the values of these coefficients, it can be concluded again that the variables had greater explanatory power at the hyperlocal scale; hence, they were included in the presented results. Furthermore, tree canopy, building density and sun-exposure had the strongest influence on $\Delta\text{ST-AT}$. The greatest impact was observed in the afternoon sun-exposure values in SHAP and Split, with building density surpassing them in Gain. This means that afternoon sun-exposure is a strong overall explanatory variable for $\Delta\text{ST-AT}$. The same can be said about building density and canopy within a sample spot: even though these do not have the highest values, they show rather high results in all three analyses. The beeswarm plots of the SHAP-values show that the amount of visible areas exposed to the sun over longer periods of time and the higher density of built-up area increase the $\Delta\text{ST-AT}$, while the proportion of tree canopy exhibits an opposite effect. This indicates that grey urban cover contributes to surface warming, while trees help to keep the temperatures down.

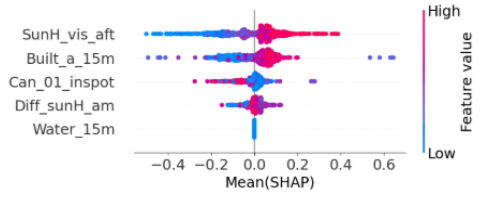
However, water within 15 m of a sample spot showed the least impact on explaining $\Delta\text{ST-AT}$. Nevertheless, as seen from the SHAP values, a high amount of water does have a negative impact on $\Delta\text{ST-AT}$, meaning water bodies provide a cooling effect. This could also suggest that the values were a result of the overall low amount of water bodies present on the hyper-local scale in the study area.

Besides the variables used as explanatory in the comparison between XGBoost and GPBoost, during this test, another parameter was added – the difference between visible sun hours in the afternoon and morning. The results of both tests are similar, with the models without this variable having slightly higher R^2 and slightly lower errors. Nevertheless, having this variable is intended to add information about accumulated heat in the areas, i.e., to test whether an extended sun-exposure period would have a stronger impact on the $\Delta\text{ST-AT}$ in the afternoon. For more details, please refer to Paper 2.

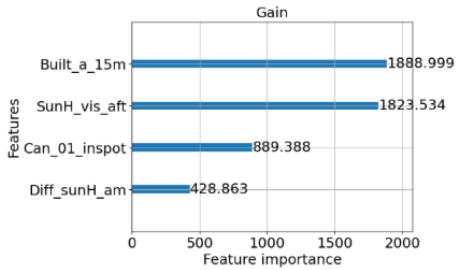
Sample spots Model 1 (SHAP bars)



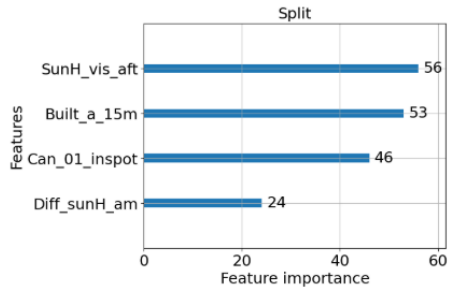
Sample spots Model 1 (beeswarm)



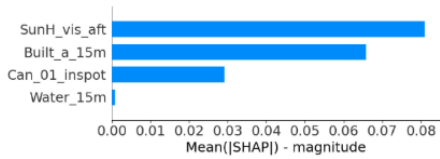
Variable importance bar (gain)



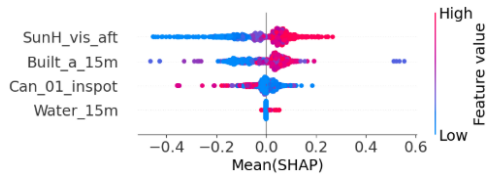
Variable importance bar (split)



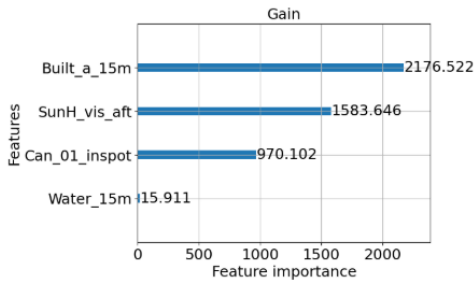
Sample spots Model 2 (SHAP bars)



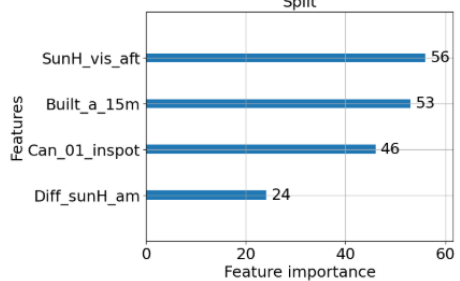
Sample spots Model 2 (beeswarm)



Variable importance bar (gain)



Variable importance bar (split)



Sample spots Model 1: $R^2 = 0.853$, RMSE = 0.582, MSE = 0.339, MAE = 0.321

Sample spots Model 2: $R^2 = 0.849$, RMSE = 0.590, MSE = 0.349, MAE = 0.321

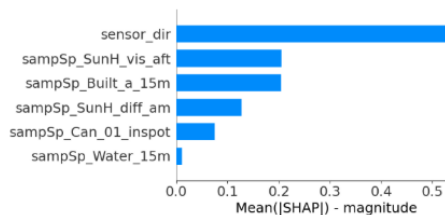
Figure 8. Results from the two best models (Model 1 and Model 2) explaining $\Delta ST-AT$ within the sample spots, using GPBoost.

3.2.3 Analysing observation points with GPBoost

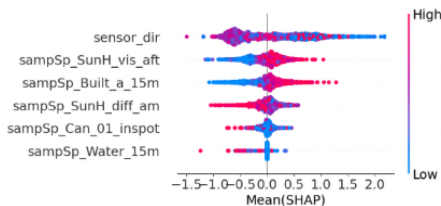
Models trained on the pre-processed datapoints achieved results similar to those trained on the sample spots, but with higher R^2 and error values. One of the variables added to the models with datapoints was sensor direction, representing a most likely bearing angle of 90° from the direction of the sensor movement, estimated by map-matching and repositioning of the measurements. Since the sun-exposure hours variable included only the ground share of the area potentially measured by the DS platforms, sensor direction was expected to provide insights into the level of sun-exposure of facades and other vertical structures captured by the IR sensor.

Furthermore, the models for the datapoints showed a more pronounced impact of the difference in the amount of sun hours between the afternoon and the morning. The results showed that areas that were most likely exposed exclusively in the afternoon tended to be cooler, possibly due to the prior period of heat relief. On the other hand, areas with the opposite type of exposure (more sun hours in the morning than in the afternoon) tended to have higher $\Delta ST-AT$ values. Lastly, the amount of tree canopy showed a trend of cooling the areas: denser canopy was associated with smaller differences between temperatures.

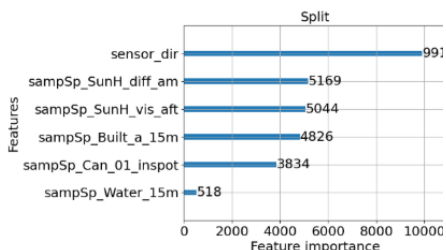
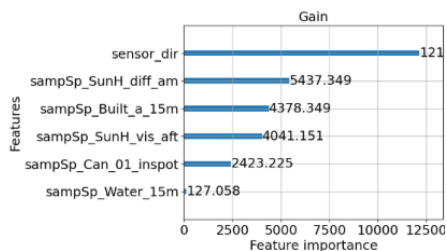
Observation points Model 1 (SHAP bars)



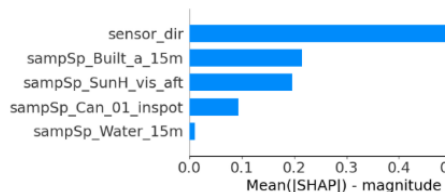
Observation points Model 1 (beeswarm)



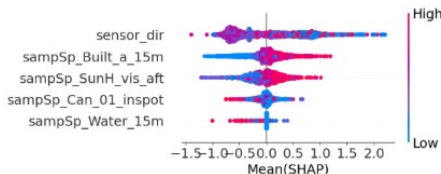
Variable importance bar



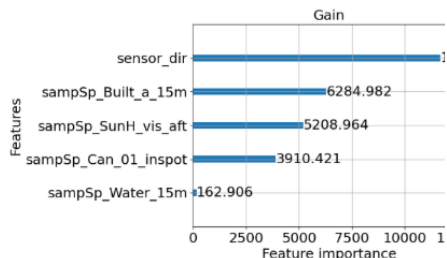
Observation points Model 2 (SHAP bars)



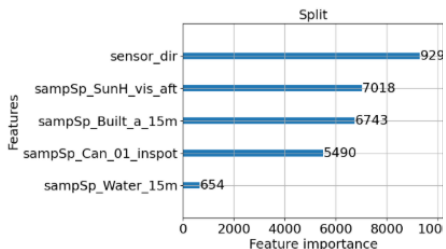
Observation points Model 2 (beeswarm)



Variable importance bar (gain)



Variable importance bar (split)



Observation points Model 1: $R^2 = 0.818$, RMSE = 0.970, MSE = 0.941, MAE = 0.651

Observation points Model 2: $R^2 = 0.816$, RMSE = 0.975, MSE = 0.951, MAE = 0.654

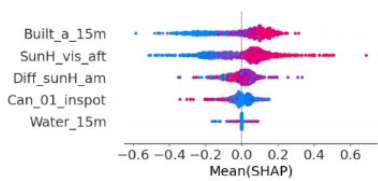
Figure 9. Results from the two best models (Model 1 and Model 2) explaining $\Delta ST-AT$ of the raw observation points, using GPBoost.

3.2.4 Comparing models with and without tree shadows

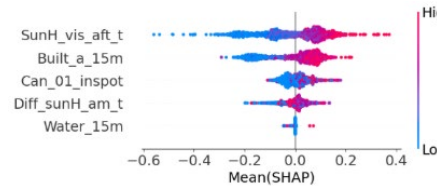
As the final step of the analyses, the models were run with sun-exposure values that included tree shadows. From these models' results, it is possible to observe the trees' shadowing effect, as shown in Figure 10. The variant without tree shadows shows a clear SHAP-value pattern: larger amounts of tree canopy mitigate the differences between surface and air temperatures. At the same time, the other model, which includes tree shadows, shows a mixed response, with changes in a substantial number of observations, with higher tree canopy values exhibiting a seemingly warming effect. Other observations exhibited the opposite pattern, where a dense canopy may cool down due to effects beyond shading alone, such as evapotranspiration.

Sample spots

Sun-hours: shadows from DEM and buildings



Sun-hours: shadows from DEM, buildings and trees

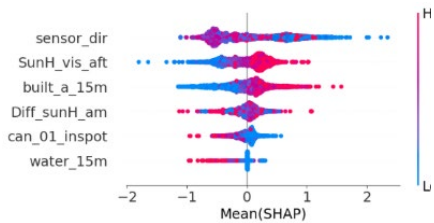


Sample spots model (no tree shadows): $R^2 = 0.844$, RMSE = 0.600, MSE = 0.360, MAE = 0.347

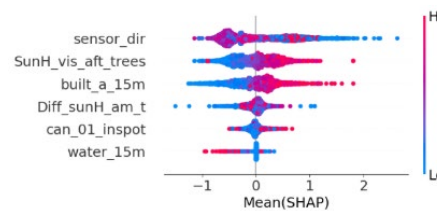
Sample spots model with tree shadows: $R^2 = 0.848$, RMSE = 0.592, MSE = 0.350, MAE = 0.334

Point data

Sun-hours: shadows from DEM and buildings



Sun-hours: shadows from DEM, buildings and trees



Point data model (no tree shadows): $R^2 = 0.831$, RMSE = 0.934, MSE = 0.873, MAE = 0.636

Point data model with tree shadows: $R^2 = 0.825$, RMSE = 0.951, MSE = 0.905, MAE = 0.653

Figure 10. Comparing models with and without tree shadows for estimating sun-exposure hours.

Comparison of Hot Spot Analysis of SHAP values from each model and canopy share itself further demonstrates this pattern (see Figure 11). Extremely low values of tree canopy, cold spots, in certain open spaces in this figure, had a strong positive influence on the results of the model without tree shadows. On the other hand, a large proportion of tree canopy was attributed to a substantial negative effect in the same model. However, with tree shadows being included, most of these extremes were identified as insignificant by the Hot Spot Analysis. This is most likely linked to the tree canopy's ability to provide shading – but in certain places, depending on street orientation, width, and tree height, the shaded area might be smaller or absent during the afternoon hours.

Figure 11 (c) shows areas that were assigned the significance level of “Insignificant” in the model without tree shadows, which were labelled as either cold or hot spots for the values of the model with tree shadows. Additionally, these areas seem to span entire street segments, suggesting the effect is not a singular outlier but rather a pattern within those streets. At the same time, several data points were identified as cold and hot spots in both models. These are rarer than the other two groups, but they are still present within the output, showing either that the model did not capture the shadowing effect here or that, in these areas, the trees had additional cooling effects, such as evapotranspiration.

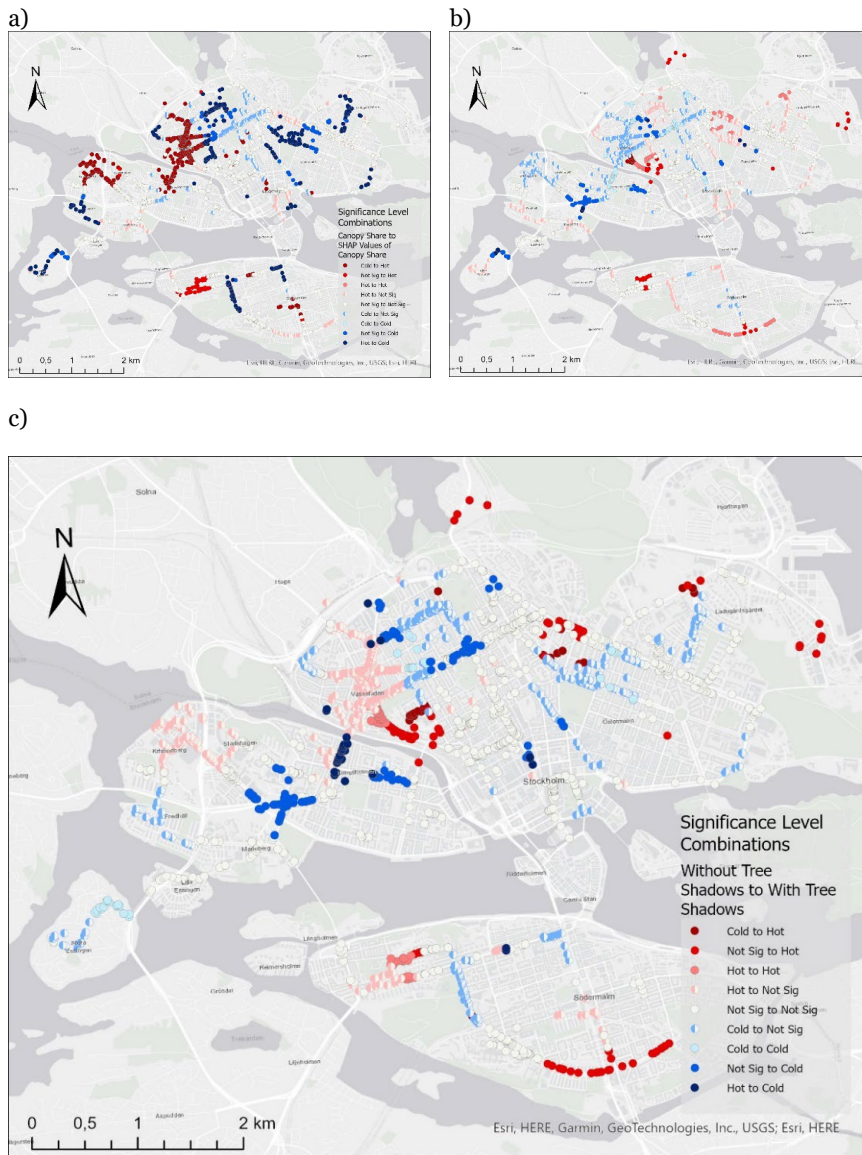


Figure 11. Comparison of Hot Spot Analyses a) shows the relation between hot and cold spots from the local tree canopy share and SHAP values from the GPBoost model without tree shadows. Comparison of Hot Spot Analyses b) shows the relation between hot and cold spots from the local canopy share and SHAP values from the GPBoost model with tree shadows included. Comparison of Hot Spot Analyses c) shows the relation between hot and cold spots from SHAP values from the GPBoost model without tree shadows and SHAP values from the GPBoost model with tree shadows included.

4 Discussion

4.1 Comparisons of temperature data sources

In this study, the correlation between T_{air} measured by DS platforms and WS was high, and they both followed the same pattern of air temperature changes and fluctuations over the course of the first case study. Nevertheless, DS T_{air} was generally higher than WS T_{air}. This could be attributed to several factors related to the data-collection specifics of each method. First, DS T_{air} could be affected by the heat produced by the vehicles on which the sensors were mounted. Even though the data were filtered by an estimated vehicle speed to ensure the DS platforms received sufficient airflow, it is possible that this effect would not have been fully negated. Second, the air sensors were placed at different heights: for the DS platform, approximately 1.5m above road level, whilst for the weather station, 2m. Moreover, one of the analysed stations was located on a rooftop, further affecting the mean difference in temperature recordings. In addition, the WS are spread out across the city, with each placed a few kilometres apart. In contrast, the DS platforms continuously measured every few seconds, potentially capturing hyperlocal variations in T_{air}. This is supported by another study, which found that T_{air} from sensors mounted on bicycles was generally higher than values from WS, with a standard deviation of $\pm 0.83^{\circ}\text{C}$ (Ziter et al., 2019).

In the case of T_{surf} compared to WS T_{air}, the difference is even higher (mean value for all hours is 2.20°C , and for morning hours, 3.96°C). While partially this could be due to the same reasons as in the case of T_{air}, most likely the discrepancy was caused by the nature of T_{surf} itself. T_{surf} has a strong connection to the immediate land cover. The amount of heat stored, reflected and emitted by a certain type of surface directly impacts T_{surf} (Oke et al. 2017).

Furthermore, when DS T_{surf} was analysed against LST derived from Landsat 8, most measurements within the same spatio-temporal window showed a strong correlation. However, DS T_{surf} was, on average, 3.3°C higher. Additionally, several outliers were identified (Figure 5). It is important to note here, that these outliers were from the same area and same side of the street, where facades were more exposed to the sun.

Another interesting finding was the so-called waterfront anomaly. In several studies, water bodies were quantified as natural cooling zones relative to LST (Lin et al. 2020; Wiman and Lindeberg 2022). However, as shown in Figures 3

and 4, the results of this case study point to a different conclusion: Tsurf values are higher along the waterfront than in the surrounding areas.

There are several possible explanations for this discrepancy between the results. Firstly, it was found that LST values derived from satellite imagery had, on average, higher errors than those of other land cover types (Tan et al. 2017). Moreover, some studies suggest that, despite water bodies potentially cooling areas adjacent to them, this effect is predominantly observed during the daytime, whereas at night the effect could be of the opposite nature (Gunawardena et al. 2017, Ampatzidis and Kershaw 2020). In addition, the same study found that during late summer, water bodies were more likely to exhibit warming. Given that this case study focused on late July and August, and on the morning hours, it is possible that the same effect was observed here.

4.2 Hot and cool zones related to greenery and grey structures

By applying multiple regression to analyse the SEH index, with SVF and GVF as explanatory variables, it was possible to explain 39.8% and 51.3% of the variation for all sample spots and for high-density spots, respectively. The SEH index was developed to include the effects of sun exposure. In the case of Paper 1, shadows were calculated from DEM and buildings only, so that the shading provided by the tree canopy would be captured by the GVF variable instead.

While the first paper focused on all hours and morning hours (including the transition from night to morning), Paper 2 shifted the focus to investigating the significance of tree canopy during midday. This change allowed to highlight the importance of greenery in obscuring surfaces from getting heated by the sun, i.e. greenery's shading properties. Due to that, denser tree canopy areas were identified as having the highest impact on surface temperature, which is in line with other studies (Ziter et al. 2019).

Moreover, since evapotranspiration is attributed to photosynthesis, the cooling abilities of trees would be the strongest when the sun is up. Despite several studies reporting on the exclusive significance of large green areas, such as parks, with diverse green cover, e.g. trees, bushes and grass (Branny et al. 2025; Zardo et al. 2017), in Paper 2, several areas identified as cold spots per SHAP value were not adjacent to parks. This could be due to either the presence of other types of greenery in those places or to the size and density of the tree canopy within the sampled radii.

Therefore, there is a need for further investigation into the importance of tree canopy in urban areas, including the effects of various types of greenery

alongside tree height, quantity, and species. The latter would provide information on the potential transmissivity of the tree canopy. In addition, in the future, species-specific data could support the transition to greenery tailored solutions to provide certain ecosystem services, including urban heat mitigation. Together, this could prove to be insightful for city planners with an opportunity for the development of more diverse and nuanced tools for mitigating extreme heat. These tools could possibly be designed for hyper-local specific challenges.

4.3 The DS approach for analysing UHI related to greenery

Using DS platforms for opportunistic data collection enabled higher spatio-temporal granularity than satellite imagery. While RS data is invaluable for larger-scale analysis over longer periods of time, it cannot assess a more detailed image of surface heat distribution across urban areas (Kim and Brown 2021a; Mirzaei 2015; Schatz and Kucharik 2015; Smoliak et al. 2015).

However, there are downsides to using self-sustaining platforms. Despite high coverage across both spatial and temporal dimensions, several areas were oversampled, while others were undersampled. This calls for stricter cleaning and preprocessing methods to ensure data quality (Kumar et al. 2015; Meier et al. 2017).

4.4 Applying machine learning to spatial data

Paper 2 followed the results of the first case study and delved into a more detailed investigation of urban surface heat. The data were modelled using ML tree-boosting algorithms (XGBoost and GPBoost) at different scales and using not only sample spots but also point data as an additional unit of assessment. Moreover, the difference between DS Tsurf and WS Tair was used as the dependent variable. The results illustrate a similar pattern, with the models having higher explanatory power on a hyper-local scale. GPBoost had, on average, a better performance than XGBoost, which is in line with other studies that compared these models when applied to spatio-temporal data (Wu et al. 2023).

In general, water bodies were the weakest variable across all models. However, SHAP values show that a high share of water bodies has a negative impact on Δ ST-AT. This result is the opposite to Paper 1. Nevertheless, since the study reported in Paper 2 covered the entire summer period, while Paper 1 focused on the later part of the summer, the waterfront anomaly should be investigated further, potentially by analysing summer months or weeks separately.

In addition, a comparison between GPBoost models with and without tree shadows provided insight into the shadowing effect from trees and its spatial distribution. Also, these effects showed to be very complex, so when the shadowing effect of tree canopy was accounted for, a very mixed effect of the presence of tree canopy remained. Further investigation is needed to understand these relationships.

5 Conclusions

This thesis investigated urban heat patterns in Stockholm using opportunistic drive-by sensing for data collection and novel ML techniques addressing, in particular, spatio-temporal and non-linear relationships. The analyses focused on interactions among urban form, tree canopy, water bodies, and surface temperature at street level, across the urban landscape.

The results show that high-resolution mobile sensing can capture substantial hyperlocal variability in both air and surface urban heat, which is difficult to detect with conventional weather stations or satellite-based observations alone. Despite several disadvantages, the method produced promising, detailed output. In this way, the study demonstrates the value of DS as a complementary method for urban climate research within the urban canopy layer.

The comparison of data sources showed that drive-by measurements of air temperature followed temporal patterns similar to those of weather stations, whereas surface temperature showed greater spatial and temporal variability. Surface temperatures were generally higher than both air temperature and satellite-derived land surface temperature, indicating that street-level measurements capture fluctuations within thermal conditions that are not fully represented by top-down or stationary approaches. This highlights the importance of the measurement perspective when assessing urban heat exposure.

The results further confirm that urban heat patterns are shaped by the combined effects of grey and green structures, both in their form and quantity. Areas characterised by higher building density and longer sun exposure tended to exhibit higher surface temperature differences, whereas the tree canopy showed a consistent cooling effect. The inclusion of sun exposure substantially improved explanatory power of the models, underlining the importance of urban geometry and shading processes in shaping local thermal conditions.

The analyses also suggest that the cooling influence of trees is not limited to the canopy: it may be linked to street morphology and the presence of other types of greenery.

Methodologically, the thesis demonstrates that tree-boosting machine learning models are effective for analysing complex, non-linear surface heat patterns in urban environments. Moreover, ML modelling approaches that integrate statistical components for analysing spatial dependencies have shown greater promise. In particular, GPBoost outperformed XGBoost, suggesting clear benefits of combining the two techniques for analysing highly variable environmental data. The strongest explanatory relationships were found at the hyperlocal scale, indicating that fine-resolution analyses are essential for understanding surface heat conditions relevant to human exposure.

Overall, this thesis contributes both methodologically and empirically to urban climate research by demonstrating how opportunistic sensing and spatial machine learning can improve the analysis of urban heat. The findings provide valuable insights for climate-sensitive urban planning and support the development of targeted heat-mitigation strategies through vegetation, shading, and urban design.

References

- Arnfield, A., 2003. Two decades of urban climate research: A review of turbulence, exchanges of energy and water, and the urban heat island. *International Journal of Climatology* 23: 1-26.
- Azevedo, J.A., Chapman, L., Muller, C.L., 2016. Quantifying the Daytime and Night-Time Urban Heat Island in Birmingham, UK: A Comparison of Satellite Derived Land Surface Temperature and High Resolution Air Temperature Observations, Remote Sensing.
- Bechtel, B., Zakšek, K., Oßenbrügge, J., Kaveckis, G., Böhner, J., 2017. Towards a satellite based monitoring of urban air temperatures. *Sustainable cities and society* 34: 22-31.
- Branny, A., Andersson, E., McPhearson, T., 2025. Micro-climate of nature-based solutions in stockholm royal seaport. *Nature-Based Solutions* 7: 100206.
- Burkhard, B., Kroll, F., Nedkov, S., Müller, F., 2012. Mapping ecosystem service supply, demand and budgets. *Ecological Indicators* 21: 17-29.
- Bärring, L., Mattsson, J.O., Lindqvist, S., 1985. Canyon geometry, street temperatures and urban heat island in malmö, sweden. *Journal of Climatology* 5: 433-444.
- Chapman, L., Bell, C., Bell, S., 2017. Can the crowdsourcing data paradigm take atmospheric science to a new level? A case study of the urban heat island of London quantified using Netatmo weather stations. *International Journal of Climatology* 37: 3597-3605.
- Clarke, J.F., 1972. Some effects of the urban structure on heat mortality. *Environmental Research* 5: 93-104.
- Cummings, L.E., Stewart, J.D., Reist, R., Shakya, K.M., Kremer, P., 2021. Mobile Monitoring of Air Pollution Reveals Spatial and Temporal Variation in an Urban Landscape. *Frontiers in Built Environment* 7.
- de Souza, P., Anjomshoa, A., Duarte, F., Kahn, R., Kumar, P., Ratti, C., 2020. Air quality monitoring using mobile low-cost sensors mounted on trash-trucks: Methods development and lessons learned. *Sustainable Cities and Society* 60: 102239.
- Depecker, P., Menezo, C., Virgone, J., Lepers, S., 2001. Design of buildings shape and energetic consumption. *Building and Environment* 36: 627-635.
- Dorman, M., Erell, E., Vulkan, A., Kloog, I., 2019. shadow: R Package for Geometric Shadow Calculations in an Urban Environment. *R J.* 11: 287.

- Earth Resources, O., Science, C., 2020. Landsat 8-9 Operational Land Imager / Thermal Infrared Sensor Level-2, Collection 2.
<http://dx.doi.org/10.5066/P9OGBGM6>,
- Elhishi, S., Elashry, A.M., El-Metwally, S., 2023. Unboxing machine learning models for concrete strength prediction using XAI. *Scientific Reports* 13: 19892.
- ESA, 2022. Sentinel-3. European Space Agency,
<https://sentinels.copernicus.eu/web/sentinel/missions/sentinel-3>,
- Greene, C.S., Millward, A.A., 2017. Getting closure: The role of urban forest canopy density in moderating summer surface temperatures in a large city. *Urban Ecosystems* 20: 141-156.
- Gunawardena, K.R., Wells, M.J., Kershaw, T., 2017. Utilising green and bluespace to mitigate urban heat island intensity. *Science of the Total Environment* 584: 1040-1055.
- Hao, M., Liu, X., Li, X., 2025. Quantifying heat-related risks from urban heat island effects: A global urban expansion perspective. *International Journal of Applied Earth Observation and Geoinformation* 136: 104344.
- He, C., Kim, H., Hashizume, M., Lee, W., Honda, Y., Kim, S.E., Kinney, P.L., Schneider, A., Zhang, Y., Zhu, Y., Zhou, L., Chen, R., Kan, H., 2022. The effects of night-time warming on mortality burden under future climate change scenarios: a modelling study. *The Lancet Planetary Health* 6: e648-e657.
- Hu, L., Monaghan, A., Voogt, J.A., Barlage, M., 2016. A first satellite-based observational assessment of urban thermal anisotropy. *Remote Sensing of Environment* 181: 111-121.
- Keeler, B.L., Hamel, P., McPhearson, T., Hamann, M.H., Donahue, M.L., Meza Prado, K.A., Arkema, K.K., Bratman, G.N., Brauman, K.A., Finlay, J.C., 2019. Social-ecological and technological factors moderate the value of urban nature. *Nature Sustainability* 2: 29-38.
- Keesstra, S., Nunes, J., Novara, A., Finger, D., Avelar, D., Kalantari, Z., Cerdà, A., 2018. The superior effect of nature based solutions in land management for enhancing ecosystem services. *Science of The Total Environment* 610-611: 997-1009.
- Kim, S.W., Brown, R.D., 2021a. Urban heat island (UHI) intensity and magnitude estimations: A systematic literature review. *Science of The Total Environment* 779: 146389.
- Kim, S.W., Brown, R.D., 2021b. Urban heat island (UHI) variations within a city boundary: A systematic literature review. *Renewable and Sustainable Energy Reviews* 148: 111256.
- Kirschner, V., Moravec, D., Macků, K., Kozhoridze, G., Komárek, J., 2024. Comparing the Effects of Green and Blue Bodies and Urban

- Morphology on Land Surface Temperatures Close to Rivers and Large Lakes, *Land*, p. 162.
- Kraemer, R., Kabisch, N., 2022. Parks Under Stress: Air Temperature Regulation of Urban Green Spaces Under Conditions of Drought and Summer Heat. *Frontiers in Environmental Science* 10.
- Kumar, P., Morawska, L., Martani, C., Biskos, G., Neophytou, M., Di Sabatino, S., Bell, M., Norford, L., Britter, R., 2015. The rise of low-cost sensing for managing air pollution in cities. *Environment International* 75: 199-205.
- Li, W., Schmidt, S., 2024. Can spatial patterns mitigate the urban heat island effect? Evidence from German metropolitan regions. *Environment and Planning B: Urban Analytics and City Science* 51: 23998083241227500.
- Li, Z., 2022. Extracting spatial effects from machine learning model using local interpretation method: An example of SHAP and XGBoost. *Computers, Environment and Urban Systems* 96: 101845.
- Lindberg, F., Grimmond, C., 2011. The influence of vegetation and building morphology on shadow patterns and mean radiant temperatures in urban areas: model development and evaluation. *Theoretical and applied climatology* 105: 311-323.
- Lindberg, F., Grimmond, C., Gabey, A., Huang, B., CW, K., T, S., N, T., Järvi, L., Ward, H., Capel-Timms, I., Chang, Y., Jonsson, P., Krave, N., Liu, D., Meyer, D., Olofson, F., Tan, J., Wästberg, D., Xue, L., Zhang, Z., 2018. Urban Multi-scale Environmental Predictor (UMEP) - An integrated tool for city-based climate services. *Environmental Modelling and Software* 99: 70-87.
- Lüthi, S., Fairless, C., Fischer, E.M., Scovronick, N., Ben, A., Coelho, M.D.S.Z.S., Guo, Y.L., Guo, Y., Honda, Y., Huber, V., Kyselý, J., Lavigne, E., Royé, D., Ryti, N., Silva, S., Urban, A., Gasparri, A., Bresch, D.N., Vicedo-Cabrera, A.M., 2023. Rapid increase in the risk of heat-related mortality. *Nature Communications* 14: 4894.
- Maes, J., Jacobs, S., 2017. Nature-Based Solutions for Europe's Sustainable Development. *Conservation Letters* 10: 121-124.
- Meier, F., Fenner, D., Grassmann, T., Otto, M., Scherer, D., 2017. Crowdsourcing air temperature from citizen weather stations for urban climate research. *Urban Climate* 19: 170-191.
- Milojevic, A., Armstrong, B.G., Gasparri, A., Bohnenstengel, S.I., Barratt, B., Wilkinson, P., 2016. Methods to Estimate Acclimatization to Urban Heat Island Effects on Heat- and Cold-Related Mortality. *Environmental Health Perspectives* 124: 1016-1022.
- Mirzaei, P.A., 2015. Recent challenges in modeling of urban heat island. *Sustainable Cities and Society* 19: 200-206.

- Mirzaei, P.A., Haghghat, F., 2010. Approaches to study Urban Heat Island – Abilities and limitations. *Building and Environment* 45: 2192-2201.
- NASA, 2022. MODIS: Moderate resolution imaging spectroradiometer. National Aeronautics and Space Administration, <https://modis.gsfc.nasa.gov/data/>,
- Obradovich, N., Migliorini, R., Mednick, S.C., Fowler, J.H., 2017. Nighttime temperature and human sleep loss in a changing climate. *Science Advances* 3: e1601555.
- Oke, T.R., 1976. The distinction between canopy and boundary-layer urban heat islands. *Atmosphere* 14: 268-277.
- Oke, T.R., 2004. Initial guidance to obtain representative meteorological observations at urban sites. Report No. 81, WMO/TD No. 1250, World Meteorological Organisation, Geneva, 51 pp.
- Oke, T.R., Mills, G., Christen, A., Voogt, J.A., 2017. *Urban climates*. Cambridge University Press.
- Padarian, J., McBratney, A.B., Minasny, B., 2020. Game theory interpretation of digital soil mapping convolutional neural networks. *SOIL* 6: 389-397.
- Quaranta, E., Dorati, C., Pistocchi, A., 2021. Water, energy and climate benefits of urban greening throughout Europe under different climatic scenarios. *Scientific Reports* 11: 12163.
- Rodríguez, M.V., Melgar, S.G., Márquez, J.M.A., 2022. Assessment of aerial thermography as a method of in situ measurement of radiant heat transfer in urban public spaces. *Sustainable Cities and Society* 87: 104228.
- Roth, M., 2013. Urban heat islands, in: Fernando, H.J. (ed.), *Handbook of Environmental Fluid Dynamics: Systems, Pollution, Modeling, and Measurements*, vol. Volume two. Taylor and Francis, Boca Raton, pp. 143-162.
- Roth, M., Oke, T., Emery, W., 1989. Satellite-derived urban heat islands from three coastal cities and the utilization of such data in urban climatology. *International Journal of Remote Sensing - INT J REMOTE SENS* 10: 1699-1720.
- Santamouris, M., 2018. *Minimizing energy consumption, energy poverty and global and local climate change in the built environment: innovating to zero: causalities and impacts in a zero concept world*. Elsevier.
- Santamouris, M., Cartalis, C., Synnefa, A., Kolokotsa, D., 2015. On the impact of urban heat island and global warming on the power demand and electricity consumption of buildings—A review. *Energy and buildings* 98: 119-124.
- Santamouris, M., Ding, L., Osmond, P., 2019. Urban Heat Island Mitigation, in: Newton, P., Prasad, D., Sproul, A., White, S. (eds.), *Decarbonising*

- the Built Environment: Charting the Transition. Springer Singapore, Singapore, pp. 337-355.
- Schatz, J., Kucharik, C.J., 2015. Urban climate effects on extreme temperatures in Madison, Wisconsin, USA. *Environmental Research Letters* 10: 094024.
- Schwarz, N., Schlink, U., Franck, U., Großmann, K., 2012. Relationship of land surface and air temperatures and its implications for quantifying urban heat island indicators—An application for the city of Leipzig (Germany). *Ecological Indicators* 18: 693-704.
- SEPA, 2018. Nationella marktäckedata [National Land Cover Data]. Swedish Environmental Protection Agency, <https://www.naturvardsverket.se/verktyg-och-tjanster/kartor-och-karttjanster/nationella-marktackedata/>,
- Shen, P., Zhao, S., Zhou, D., Lu, B., Han, Z., Ma, Y., Wang, Y., Zhang, C., Shi, C., Song, L., Pan, Z., Li, Z., Liu, S., 2024. Surface and canopy urban heat island disparities across 2064 urban clusters in China. *Sci Total Environ* 955: 177035.
- Sheng, L., Tang, X., You, H., Gu, Q., Hu, H., 2017. Comparison of the urban heat island intensity quantified by using air temperature and Landsat land surface temperature in Hangzhou, China. *Ecological Indicators* 72: 738-746.
- Sigrist, F., 2021. Gaussian Process Boosting.
- Sigrist, F., 2024. Gaussian Process Boosting. arXiv.
- Smoliak, B.V., Wallace, J.M., Lin, P., Fu, Q., 2015. Dynamical Adjustment of the Northern Hemisphere Surface Air Temperature Field: Methodology and Application to Observations. *Journal of Climate* 28: 1613-1629.
- Song, B., Park, K., 2020. Verification of accuracy of unmanned aerial vehicle (UAV) land surface temperature images using in-situ data, Remote Sensing.
- Streutker, D.R., 2002. A remote sensing study of the urban heat island of Houston, Texas. *International Journal of Remote Sensing* 23: 2595-2608.
- Tan, K., Liao, Z., Du, P., Wu, L., 2017. Land surface temperature retrieval from Landsat 8 data and validation with geosensor network. *Frontiers of Earth Science* 11: 20-34.
- Theeuwes, N.E., Steeneveld, G.J., Ronda, R.J., Holtslag, A.A., 2017. A diagnostic equation for the daily maximum urban heat island effect for cities in northwestern Europe. *International Journal of Climatology* 37: 443-454.
- Tuholske, C., Caylor, K., Funk, C., Verdin, A., Sweeney, S., Grace, K., Peterson, P., Evans, T., 2021. Global urban population exposure to extreme heat.

- Proceedings of the National Academy of Sciences of the United States of America 118: e2024792118.
- USGS, 2023. Landsat 8. United States Geological Survey, <https://www.usgs.gov/landsat-missions/landsat-8>,
- van Someren, E.J.W., 2003. Thermosensitivity of the circadian timing system. *Sleep Biol. Rhythms* 1.
- Venter, Z.S., Chakraborty, T., Lee, X., 2021. Crowdsourced air temperatures contrast satellite measures of the urban heat island and its mechanisms. *Science Advances* 7: eabb9569.
- Venter, Z.S., Krog, N.H., Barton, D.N., 2020. Linking green infrastructure to urban heat and human health risk mitigation in Oslo, Norway. *Science of The Total Environment* 709: 136193.
- Visintin, C., Garrard, G.E., Weisser, W.W., Baracco, M., Hobbs, R.J., Bekessy, S.A., 2025. Designing cities for everyday nature. *Conservation Biology* 39: e14328.
- Voogt, J.A., Oke, T.R., 2003. Thermal remote sensing of urban climates. *Remote Sensing of Environment* 86: 370-384.
- Wang, H., Huang, Z., Guo, H., Yin, G., Bao, Y., Zhou, X., Gao, Y., Li, L., 2026. GWRBoost: A Geographically Weighted Gradient Boosting Framework for Enhanced Explainable Quantification of Spatially Varying Relationships. *Annals of the American Association of Geographers*: 1-19.
- Wong, N.H., Tan, C.L., Kolokotsa, D.D., Takebayashi, H., 2021. Greenery as a mitigation and adaptation strategy to urban heat. *Nature Reviews Earth & Environment* 2: 166-181.
- Wu, J., Jia, P., Feng, T., Li, H., Kuang, H., 2023. Spatiotemporal analysis of built environment restrained traffic carbon emissions and policy implications. *Transportation Research Part D: Transport and Environment* 121: 103839.
- Yang, X., Li, Y., 2015. The impact of building density and building height heterogeneity on average urban albedo and street surface temperature. *Building and Environment* 90: 146-156.
- Zardo, L., Geneletti, D., Pérez-Soba, M., Van Eupen, M., 2017. Estimating the cooling capacity of green infrastructures to support urban planning. *Ecosystem Services* 26: 225-235.
- Zhang, P., Bounoua, L., Imhoff, M., Wolfe, R., Thome, K., 2014. Comparison of MODIS Land Surface Temperature and Air Temperature over the Continental USA Meteorological Stations. *Canadian Journal of Remote Sensing* 40: 110-122.
- Zhang, P., Jia, Y., Shang, Y., 2022. Research and application of XGBoost in imbalanced data. *International Journal of Distributed Sensor Networks*.

- Zhao, B., Yu, L., Wang, C., Shuai, C., Zhu, J., Qu, S., Taiebat, M., Xu, M., 2021. Urban Air Pollution Mapping Using Fleet Vehicles as Mobile Monitors and Machine Learning. *Environmental Science & Technology* 55: 5579-5588.
- Zhao, X., Luo, Y., He, J., 2020. Analysis of the thermal environment in pedestrian space using 3D thermal imaging, *Energies*.
- Zhao, Y., Chen, Y., Li, K., 2025. Revealing the impacts of 3D urban morphology on surface temperature considering geometry heterogeneity, component contribution, and scale effect. *Sustainable Cities and Society* 119: 106093.
- Ziter, C.D., Pedersen, E.J., Kucharik, C.J., Turner, M.G., 2019. Scale-dependent interactions between tree canopy cover and impervious surfaces reduce daytime urban heat during summer. *Proceedings of the National Academy of Sciences* 116: 7575-7580.